

Highly efficient superconducting diode effect in unconventional p -wave magnets

Igor de M. Froldi and Hermann Freire
Instituto de Física, Universidade Federal de Goiás, 74.690-900, Goiânia-GO, Brazil

We investigate the emergence of superconducting phases, both with zero and finite Cooper-pair center of mass momenta, in recently proposed unconventional p -wave magnets. As a consequence, we find that, while these magnetic phases are in principle compatible with a conventional pairing state at zero field, a Fulde-Ferrell phase can generally be promoted as the leading instability under the application of a finite magnetic field. Interestingly, by calculating the efficiency of the superconducting diode effect of this finite momentum pairing state via a Ginzburg-Landau theory, we uncover that a high efficiency can be obtained in these systems for experimentally relevant spin splittings. Therefore, our prediction reveals that the experimental discovery of these new materials represents a promising platform for the construction of energy-efficient logic circuits that can potentially be used, e.g., in the fields of classical and quantum computing.

Introduction— Unconventional magnetism that features spin-split band structures with zero magnetization in the absence of magnetic field and spin-orbit coupling is a central research topic nowadays in condensed matter physics. One notable example is the recently discovered altermagnetism (AM) [1–4] that consists of a newly classified collinear magnetic state, which breaks the time-reversal symmetry \mathcal{T} , but does not exhibit net magnetization due to a compensating discrete rotational symmetry. As a result, it generates even-parity spin splittings (d -, g -, or i -wave) with many AM materials being subsequently discovered in the literature (see, e.g., Refs. [5–10]). One of the motivations underlying this quest is that AM compounds are expected to lead to important applications in the field of spintronics [11–14]. Shortly thereafter, inspired by this remarkable discovery, another unconventional magnetic state was proposed [15] for non-collinear coplanar magnetic moments, which instead displays an odd-parity spin splitting [15–24] (p -, f -, or h -wave). In the latter systems, the time-reversal \mathcal{T} is preserved but the inversion symmetry \mathcal{I} is broken. In addition, the existence of a composite symmetry $\mathcal{T}\tau$ (where τ is a translation operator) protects the odd-parity spin polarization, leading to a zero net magnetization. Some examples of compounds that might display unconventional p -wave magnetism (UPM) are, e.g., NiI_2 [25], CeNiAsO [15, 18], and $\text{Gd}_3(\text{Ru}_{1-x}\text{Rh}_x)_4\text{Al}_{12}$ [26], while higher-order h -wave magnetism has recently been proposed in the context of some iron-based materials [18, 19].

Furthermore, unconventional superconductivity (SC) arising as a result of proximity to magnetic phases is another topic of immense interest in the field, since a clear interconnection between these phases appears in many examples of strongly correlated quantum materials. Here, we will focus specifically on the investigation of the impact of UPM on possible emergent unconventional SC phases. A similar analysis has been initiated in recent years regarding the effect of AM on new pairing states, with several interesting phenomena being predicted in a wide range of works including, e.g., topological superconductivity [27–30], pair-density waves (PDW) [31–35], other unconventional SC phases [27, 36–42], the study of the superconducting diode effect (SDE) [33, 43–48], etc. However, an analogous comprehensive investigation has not yet been performed in the context of UPM, except from a few re-

cent works that studied, e.g., proximity effects of these new magnetic materials with superconductors [49–51], the analysis of the coexistence of conventional superconductivity with UPM [52], and the computation of transport properties associated with SC in these systems [53], among other examples (see, e.g., Ref. [24]).

In this work, we derive a Ginzburg-Landau (GL) theory for the study of both zero- and finite-momentum superconductivity that appear in unconventional odd-parity magnets. Our analysis will concentrate on the investigation of nonreciprocal transport that takes place specifically in emergent PDW phases. In this regard, we will study the SDE efficiency systematically as a function of the UPM spin splitting, temperature, and magnetic field. Consequently, we find, quite remarkably, that UPM materials are expected to yield highly efficient diode effects for experimentally relevant parameters, which could provide a promising pathway for advancing a new platform for energy-efficient electronic devices that can be ultimately used in the fields of classical and quantum computing, and in new superconducting sensors as well [48].

Model and method— We begin our analysis with a two-dimensional (2D) low-energy model that describes a p -wave itinerant magnet given by:

$$H_0 = \sum_{\mathbf{k}, s, s'} \psi_{\mathbf{k}, s}^\dagger [\mathbb{1} \xi_{\mathbf{k}} + \lambda \mathbf{g}_{\mathbf{k}} \cdot \boldsymbol{\sigma} + \mathbf{B} \cdot \boldsymbol{\sigma}]_{ss'} \psi_{\mathbf{k}, s'}, \quad (1)$$

where $\psi_{\mathbf{k}s}^\dagger$ ($\psi_{\mathbf{k}s}$) creates (annihilates) an electron with momentum \mathbf{k} and spin projection $s = \uparrow, \downarrow$, $\xi_{\mathbf{k}} = c_0 \mathbf{k}^2 - \mu$, $\boldsymbol{\sigma} = (\sigma_x, \sigma_y, \sigma_z)$ is the vector of Pauli matrices, $\mathbb{1}$ is the identity matrix, $c_0 = 1/(2m)$, μ is the chemical potential, and m represents the effective mass. The strength of the spin splitting is parametrized by λ with the form factor given by $\mathbf{g}_{\mathbf{k}}$, which displays p -wave symmetry (e.g., $\mathbf{g}_{\mathbf{k}} \sim k_x \hat{\mathbf{z}}$ in the vicinity of the Γ point). Since the p -wave spin splitting satisfies $\mathbf{g}_{-\mathbf{k}} = -\mathbf{g}_{\mathbf{k}}$, it preserves time-reversal symmetry \mathcal{T} . However, inversion symmetry \mathcal{I} is broken and, therefore, this term is similar from this point of view to a Rashba spin-orbit coupling (we point out though that the former can be significantly larger than the latter due to its exchange interaction origin [15]). The UPM form factor splits the bands at the Fermi level as shown schematically in Fig. 1. Moreover, we investigate here the effects of a uniform out-of-plane magnetic field $\mathbf{B} = B_z \hat{\mathbf{z}}$. Throughout

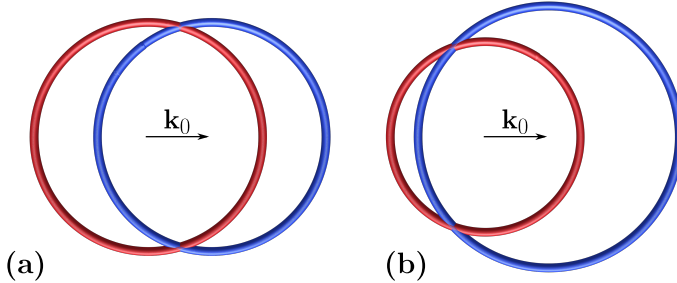


FIG. 1. Schematic representation of the spin splitting of the Fermi surfaces in a UPM, for (a) zero magnetic field and (b) an out-of-plane magnetic field given by $\mathbf{B} = B_z \hat{\mathbf{z}}$. The spin polarization of the Fermi surfaces displayed by the present model only assumes one of the values $\langle \sigma_z \rangle = \pm \hbar/2$, indicated, respectively, by the colors red and blue in the FS. Note that the Fermi surfaces are always displaced from the center of the zone for a finite λ , indicated by the wavevector $\mathbf{k}_0 = 2 \frac{m\lambda}{\hbar^2} \hat{\mathbf{x}}$. The nodes of the FS are present up to a critical out-of-plane field given by $B_c = \pm |\lambda| \sqrt{\frac{2m\mu}{\hbar^2}}$, where μ is the chemical potential. Also, we point out that any infinitesimal in-plane magnetic field leads instead to nodeless Fermi surfaces.

in this work, we will use units such that $\hbar = k_B = e = 1$ in all expressions. Finally, we normalize the couplings at the noninteracting Fermi surface (FS), such that $\langle |\mathbf{g}_{\mathbf{k}}|^2 \rangle_{\text{FS}} = 1$, where $\langle \dots \rangle_{\text{FS}} = \int_0^{2\pi} (\dots) d\theta / 2\pi$.

The pairing instabilities in this model can be analyzed by adding to Eq. (1) a standard BCS-type attractive interaction given by a general term:

$$H_{\text{int}} = \frac{1}{2} \sum_{\substack{\mathbf{k}, \mathbf{k}', \mathbf{q} \\ s, s'}} V_{\mathbf{k}, \mathbf{k}'} \psi_{\mathbf{k} + \frac{\mathbf{q}}{2}, s}^\dagger \psi_{-\mathbf{k} + \frac{\mathbf{q}}{2}, s'}^\dagger \psi_{-\mathbf{k}' + \frac{\mathbf{q}}{2}, s'} \psi_{\mathbf{k}' + \frac{\mathbf{q}}{2}, s}, \quad (2)$$

where $V_{\mathbf{k}, \mathbf{k}'} < 0$ near the Fermi surface, within a range defined by a characteristic cutoff ϵ_c . For the moment, we will restrict our analysis to the possible formation of both zero- and finite-momentum spin-singlet s -wave superconductor (i.e., we will focus on the case in which $s = \uparrow$ and $s' = \downarrow$ in Eq. (2)). This choice is motivated by the fact that this scenario, most commonly assumed for phonon-mediated pairing mechanism, is a likely possibility of pair formation in the present model (see, e.g., the discussion in Ref. [52]). Consequently, we assume that $V_{\mathbf{k}, \mathbf{k}'} = -V_s d_0(\mathbf{k}) d_0(\mathbf{k}')$, where $V_s > 0$ and $d_0(\mathbf{k}) = 1$. Therefore, we will concentrate our discussion in the main text on the investigation of such s -wave pairing states in the presence of UPM, and leave the analysis of the possibility of existence of long-range interactions that can promote spin-singlet d -wave SC and spin-triplet p -wave pairing states to the Supplemental Material (SM) [54].

Next, we decouple the above interaction using mean-field theory in the singlet channel, by defining the order-parameter field self-consistently as follows:

$$\langle \psi_{-\mathbf{k} + \frac{\mathbf{q}}{2}, \downarrow} \psi_{\mathbf{k} + \frac{\mathbf{q}}{2}, \uparrow} \rangle \equiv - \sum_{\mathbf{k}, \{\mathbf{Q}\}} \delta_{\mathbf{q}, \mathbf{Q}} V_{\mathbf{k}, \mathbf{k}'}^{-1} \Delta_{\mathbf{Q}}(\mathbf{k}), \quad (3)$$

where we used the notation $\{\mathbf{Q}\}$ in the sum to make explicit the fact that the summation is discrete and takes place only on some specific values (to be determined shortly). Using the Nambu basis $\Psi_{\mathbf{k}} = (\psi_{\mathbf{k}, \uparrow}, \psi_{\mathbf{k}, \downarrow}, \psi_{-\mathbf{k}, \uparrow}^\dagger, \psi_{-\mathbf{k}, \downarrow}^\dagger)^T$, we write the complete Hamiltonian $H = H_0 + H_{\text{int}}$ in the Bogoliubov-de-Gennes (BdG) form:

$$H = \frac{1}{2} \sum_{\mathbf{k}, \mathbf{k}'} \Psi_{\mathbf{k}'}^\dagger \begin{pmatrix} \mathcal{H}_0(\mathbf{k}) \delta_{\mathbf{k}, \mathbf{k}'} & \Delta_{\mathbf{k}, \mathbf{k}'}(\mathbf{Q}) \\ [\Delta_{\mathbf{k}', \mathbf{k}}(\mathbf{Q})]^\dagger & -[\mathcal{H}_0(\mathbf{k})]^T \delta_{\mathbf{k}, \mathbf{k}'} \end{pmatrix} \Psi_{\mathbf{k}} + \sum_{\mathbf{k}, \mathbf{k}', \{\mathbf{Q}\}} V_{\mathbf{k}, \mathbf{k}'}^{-1} |\Delta_{\mathbf{Q}}(\mathbf{k}')|^2, \quad (4)$$

where a constant term has been dropped since it represents only a shift in total energy, and we have defined:

$$\Delta_{\mathbf{k}, \mathbf{k}'}(\mathbf{Q}) = \sum_{\{\mathbf{Q}\}} \Delta_{\mathbf{Q}} \left(\frac{\mathbf{k} + \mathbf{k}'}{2} \right) i \sigma_y \delta_{\mathbf{k}, \mathbf{k}' + \mathbf{Q}}. \quad (5)$$

The BdG Hamiltonian in Eq. (S5) is quadratic in the fermionic fields. Hence, these degrees of freedom can be integrated out via a path-integral formalism, which will lead to the Ginzburg-Landau (GL) free energy (for details, see the SM [54]). We parametrize the order parameter field as $\Delta_s^{(\mathbf{Q})}(\mathbf{k}) = |\Delta_s^{(\mathbf{Q})}| d_0(\mathbf{k})$, where $d_0(\mathbf{k})$ refers to the form factor already explained for the appropriate spin-singlet SC state, normalized over the Fermi surface. The resulting GL free energy up to fourth-order in the order parameter yields:

$$\mathcal{F} [\Delta^\dagger, \Delta] = \sum_{\{\mathbf{Q}\}} \left(\alpha_s(\mathbf{Q}, T) |\Delta_s^{(\mathbf{Q})}|^2 + \chi_s |\Delta_s^{(\mathbf{Q})}|^4 \right), \quad (6)$$

where we neglected, without loss of generality, the free energy in the normal state. The coefficient $\alpha_s(\mathbf{Q}, T)$ is given by a polarization bubble in the appropriate pairing channel, and describes the phase transition from the normal metal phase to the superconducting states (with either zero or finite Cooper pair momentum). By defining the effective coupling $\mathbf{g}_k^{\text{eff}} = \lambda \mathbf{g}_k + \mathbf{B}$, and using the digamma function $\psi^{(0)}(x)$ to define $\Xi(x) = \text{Re}[\psi^{(0)}(\frac{1}{2} + ix)] - \psi^{(0)}(\frac{1}{2})$, this second-order coefficient becomes:

$$\alpha_s(\mathbf{q}, T) = N_F \ln \left(\frac{T}{T_{c,s}^{(0)}} \right) + \frac{N_F}{4} \sum_{\gamma=\pm} \int_{FS} \frac{d\theta}{2\pi} d_0^2(\mathbf{k}) \left[\Xi \left(\frac{\gamma g_1 + \frac{\mathbf{q}}{2} \cdot \mathbf{v}_F}{2\pi T} \right) \left(1 + \hat{\mathbf{g}}_{\mathbf{k} + \frac{\mathbf{q}}{2}}^{\text{eff}} \cdot \hat{\mathbf{g}}_{-\mathbf{k} + \frac{\mathbf{q}}{2}}^{\text{eff}} \right) + \Xi \left(\frac{\gamma g_2 + \frac{\mathbf{q}}{2} \cdot \mathbf{v}_F}{2\pi T} \right) \left(1 - \hat{\mathbf{g}}_{\mathbf{k} + \frac{\mathbf{q}}{2}}^{\text{eff}} \cdot \hat{\mathbf{g}}_{-\mathbf{k} + \frac{\mathbf{q}}{2}}^{\text{eff}} \right) \right], \quad (7)$$

where $\hat{\mathbf{g}}_k^{\text{eff}} \equiv \mathbf{g}_k^{\text{eff}} / |\mathbf{g}_k^{\text{eff}}|$ is the unit vector along the effective coupling vector, while $g_{1,2} = (|\mathbf{g}_{\mathbf{k} + \frac{\mathbf{q}}{2}}^{\text{eff}}| \pm |\mathbf{g}_{-\mathbf{k} + \frac{\mathbf{q}}{2}}^{\text{eff}}|)/2$ denotes, respectively, the mean energy and the energy difference due to the effective coupling at different points on the Fermi surface, and $\mathbf{v}_F = k_F(\cos \theta \hat{\mathbf{x}} + \sin \theta \hat{\mathbf{y}})/m$ stands for the Fermi velocity. The coupling strength V_s in the spin-singlet channel has been absorbed in the definition of the critical temperature $T_{c,0}^{(s)}$ in the absence of spin-splitting and magnetic fields (i.e., for $\lambda = |\mathbf{B}| = 0$) defined as $T_{c,0}^{(s)} = (2e^\gamma \epsilon_c / \pi) e^{-1/(N_F V_s)}$, where $\gamma = 0.57721...$

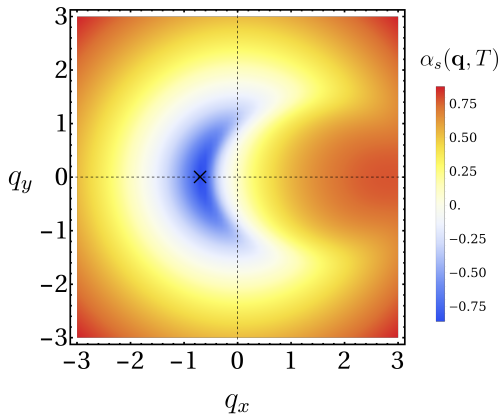


FIG. 2. Second-order GL coefficient [Eq. (6)] for the s -wave FF state in the present model. Here, we choose $\lambda/T_{c,0} = 1$, $B/T_{c,0} = 1$, and $T = 0.1T_{c,0}$. The symbol “ \times ” marks the global minimum of the GL free energy, which yields $\mathbf{Q} \approx -0.7\hat{\mathbf{x}}$ in this case. The “half-moon” pattern of this plot stems from both time-reversal and inversion symmetry breakings.

is the Euler-Mascheroni constant and N_F is the noninteracting density of states at the Fermi level. Henceforth, all temperatures and couplings will be measured w.r.t. $T_{c,0}^{(s)}$. The coefficient χ_s in Eq. (6) is derived for our microscopic model from a four-legged Feynman diagram, which is calculated for the corresponding minimizing wave vector \mathbf{Q} . Since the latter result yields a cumbersome expression, we leave its detailed explanation for the SM [54].

We are now ready to define the set denoted by $\{\mathbf{Q}\}$, e.g., in Eq. (S5). They can be extracted by minimizing the coefficient $\alpha_s(\mathbf{q}, T)$ with respect to an arbitrary momentum \mathbf{q} and temperature T , thus obtaining a temperature dependent wave vector $\mathbf{Q}(T)$, similar to that found for the case of PDW formation in electronic liquid-crystal phases [55]. We then find the corresponding critical temperature (denoted by $T_c^{(s)}$) for the transition between the normal state and the spin-singlet SC phases by solving the linearized gap equation, i.e., $\alpha_s[\mathbf{Q}(T_c^{(s)}), T_c^{(s)}] = 0$. Interestingly, we obtain that, at zero magnetic field, a UPM splitting does not generate any finite momentum pairing for spin-singlet states, which contrasts with the scenario regarding the emergence of superconductivity in altermagnets [31–35, 47].

As we switch on the magnetic field, only one stable minimum referring to a pairing phase with modulation \mathbf{Q} is found. Only the direction of \mathbf{Q} turns out to be temperature independent (for details, see SM [54]), which points along one of the antinodal directions (see Fig. 2) – again, in sharp contrast to the case of altermagnets [33, 46, 47]. This spatial modulation implies that the only finite-momentum superconducting phase that emerges in this case is a Fulde-Ferrell (FF) state [56, 57], which breaks spontaneously both time-reversal and inversion symmetries. The corresponding expression that describes the FF order parameter is then given by $\Delta_s^{\text{FF}}(\mathbf{r}) = \Delta_s^{(\mathbf{Q})} e^{i\mathbf{Q} \cdot \mathbf{r}}$. The minimization of the free energy, Eq. (6), with respect to the order parameter field

for the FF modulation is then given by:

$$\mathcal{F}_{\text{FF}}^{\min} = -\frac{\alpha_s(\mathbf{Q}, T)}{4\chi_s(\mathbf{Q}, T)}, \quad (8)$$

where the stability conditions inside the pairing state are given by $\alpha_s[\mathbf{Q}(T), T] < 0$ and $\chi_s[\mathbf{Q}(T), T] > 0$.

Phase diagram— We now turn our attention to the determination of the phase diagram associated with our effective model, which is displayed in Fig. 3(a). For $\mathbf{B} = 0$, since the UPM Hamiltonian displays explicitly only inversion symmetry breaking, a spin-singlet pairing state remains unaffected w.r.t. the increase of λ . As we switch on the magnetic field \mathbf{B} along the out-of-plane ($\hat{\mathbf{z}}$) direction, and for $\lambda = 0$, the zero momentum spin-singlet pairing state is suppressed, but only above a finite critical field. For nonzero λ and \mathbf{B} , the situation changes dramatically. Even for a small magnetic field, the increase in λ leads to the formation of an FF state, indicating that UPM is a favorable platform for the emergence of finite-momentum superconductivity in the spin-singlet channel. As \mathcal{T} -symmetry breaking terms are detrimental to spin-singlet pairs, there is a maximum B_P , which suppresses completely both zero and finite momentum pairing in this case (this is the so-called Pauli limiting field). Note that B_P is enhanced as we increase the UPM splitting λ , as indicated by the line separating the FF and the UPM phases in Fig. 3(a). This behavior is similar with the properties discussed by works on superconductivity in noncentrosymmetric materials, where an inversion-assymmetric Rashba spin-orbit coupling (SOC) also has the effect of increasing the Pauli field (see, e.g., Ref. [58]).

Intrinsic diode effect— Since the UPM effective model clearly exhibits (even for a small λ and \mathbf{B}) a spin-singlet FF pairing phase with both time-reversal and inversion symmetry breakings, nonreciprocal phenomena are naturally expected to emerge. The supercurrent associated with such a phase displayed by our effective model can be calculated via minimal coupling of the superconducting wave vector to an external vector potential \mathbf{A} using the relation $\mathbf{J}(\mathbf{q}) = -\lim_{\mathbf{A} \rightarrow 0} \nabla_{\mathbf{A}} \mathcal{F}(\mathbf{q} - 2\mathbf{A})$. Therefore, we obtain:

$$\mathbf{J}(\mathbf{q}) = -\frac{1}{2\chi_s} \alpha_s(\mathbf{q}, T) \nabla_{\mathbf{q}} \alpha_s(\mathbf{q}, T). \quad (9)$$

For nonzero λ and \mathbf{B} , the supercurrent is not only asymmetric with respect to \mathbf{q} , but can also be skewed, leading to different maximum and minimum values. These features displayed by our model naturally lead to nonreciprocal properties such as the superconducting diode effect (SDE), which refers to a phenomenon where the critical currents parallel and antiparallel to the Cooper pair momentum turn out to be unequal [48, 59–61]. By writing $\mathbf{J}(\mathbf{q}) = J(\mathbf{q})\hat{\mathbf{n}}$, we can analyze this supercurrent in fixed directions $\hat{\mathbf{n}}$ with respect to the direction of the minimizing wave vector \mathbf{Q} . Defining J_c^+ and J_c^- as, respectively, the maximum and minimum values of the supercurrent, we can evaluate the asymmetry of the supercurrent in the model by computing the SDE efficiency η given by:

$$\eta = \frac{J_c^+ - J_c^-}{J_c^+ + J_c^-}. \quad (10)$$

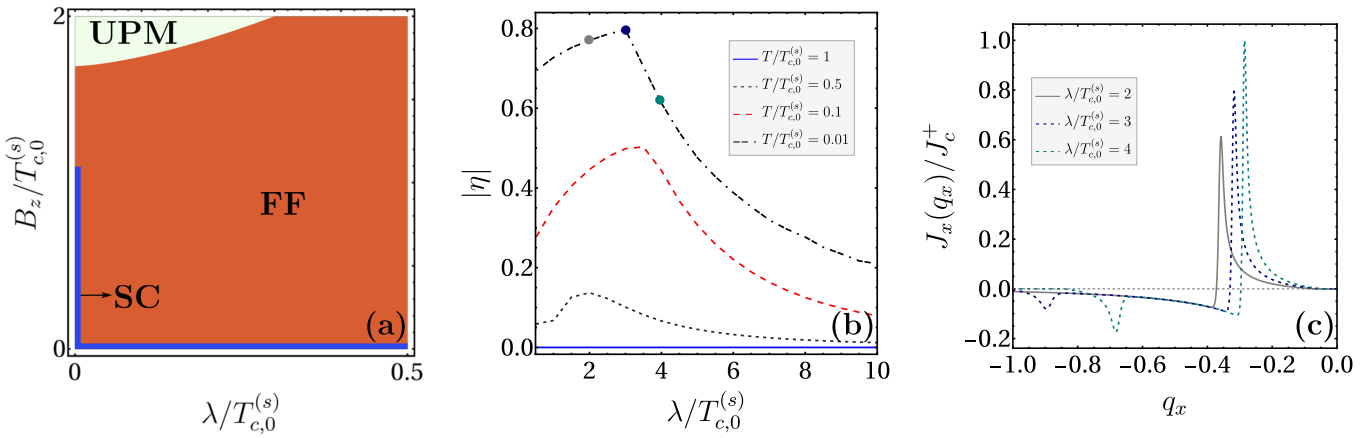


FIG. 3. (a) Schematic pairing phase diagram of B_z vs. λ in the present model. The white region denotes the UPM phase, the red region stands for the spin-singlet s -wave FF phase and the blue region corresponds to the spin-singlet s -wave zero-momentum SC phase. (b) Efficiency η of the SDE [Eq. (10)] for the FF phase with modulation along the direction of the minimizing wave vector \mathbf{Q} , as a function of the UPM spin splitting λ for a finite magnetic field such that $B_z/T_{c,0}^{(s)} = 1$. We also show the behavior of η in the model for different temperatures T . (c) Supercurrent as a function of the momentum q_x for different values of the spin splitting around the maximum of the efficiency, indicated by three circles shown in (b), at $T = 0.01T_{c,0}^{(s)}$.

In Fig. 3(b), we plot this quantity for different temperatures as a function of the UPM splitting λ for a finite magnetic field (here, we assume that $\hat{\mathbf{n}} = \hat{\mathbf{x}}$, which points along the direction of the modulation \mathbf{Q} of the FF phase – this yields the maximized SDE efficiency). Consequently, we observe that the SDE efficiency has a peak for low temperatures at an optimal splitting λ_{opt} , which can reach almost 80% of efficiency for some conveniently chosen physical parameters. We also point out that the SDE efficiency clearly exhibits a monotonically increasing behavior with decreasing temperature. As can be seen in Fig. 3(c), where the supercurrents are plotted at $T = 0.01T_{c,0}^{(s)}$ for UPM splittings λ with either smaller or larger values than this optimal point, the supercurrent starts to develop a local minimum and the variation of λ makes this a global minimum responsible for the decrease in the parameter η . We also note that the efficiency goes to zero when $\lambda = 0$, indicating that UPM is crucial to obtain a finite SDE in our model. Lastly, we mention that although these results were obtained within a GL theory, we point out that this framework, in general, gives a lower bound of this effect. For this reason, even a higher SDE efficiency in the present system is plausible beyond the GL regime (see, e.g., Ref. [43]).

Recently, density-functional-theory (DFT) calculations have predicted UPM, e.g., in the heavy-fermion compound CeNiAsO [15], and also in some iron based superconductors (see, e.g., LaFeAsO [24]). We point out that in the latter compounds, in the presence of SOC, a p -wave spin splitting is obtained along the k_x and k_y directions, while in the k_z -direction it exhibits an h -wave character. The UPM splitting λ in the iron-based superconductor was predicted to be relatively small ($\lambda \sim 10$ meV), while in the heavy-fermion case it was found to be one order of magnitude larger ($\lambda \sim 100$ meV). Our calculation indicates that, for larger ratios ($\lambda/T_{c,0}^{(s)}$), the diode effect is expected to have a higher efficiency with the application of the magnetic field

at low temperatures. Therefore, specifically for the candidate material LaFeAsO, the reported spin splitting falls within the range $\lambda \sim 1 - 10$ meV, which fits into the window of highest SDE efficiencies for the case of $T_{c,0}^{(s)} \sim 30$ K [see again Fig. 3(b)].

Before arriving at the final conclusions, we make a brief comment, for the sake of completeness, on possible emergent d -wave spin-singlet SC and p -wave pairing states in the presence of UPM within our model. For the case of d -wave SC, we have verified that the corresponding pairing phase diagram does not change qualitatively compared to the s -wave pairing scenario: for $B = 0$, we find a zero-momentum SC phase for any λ , and, as soon as both λ and \mathbf{B} are finite, we obtain that the leading instability is towards a spin-singlet d -wave FF phase, whose SDE efficiency yields smaller values than the s -wave FF case (for more details, see the SM [54]).

Regarding possible spin-triplet pairings in the model, we have investigated the instabilities associated with p -wave symmetry for both mixed-spin (i.e., chiral-type) described by the form factor vector $\mathbf{d}(\mathbf{k}) = (k_x + ik_y)\hat{\mathbf{z}}$, and equal-spin (i.e., helical-type) described by the order-parameter $\mathbf{d}(\mathbf{k}) = i(k_x\hat{\mathbf{y}} + k_y\hat{\mathbf{x}})$ [62]. For $\mathbf{B} = 0$, the chiral (mixed spin) p -wave state does not generate any finite-momentum superconductivity, while the helical (equal spin-triplet) is capable of generating PDW at zero fields with two minimizing wave vectors $\pm\mathbf{Q}$. The latter corresponds to a spatial modulation given by $\Delta_{\text{LO}}^{\text{LO}}(\mathbf{r}) = \Delta_t^{(\mathbf{Q})}e^{i\mathbf{Q}\cdot\mathbf{r}} + \Delta_t^{(-\mathbf{Q})}e^{-i\mathbf{Q}\cdot\mathbf{r}}$ (also called a Larkin-Ovchinnikov (LO) phase [57, 63]), therefore preserving both time-reversal and inversion symmetries; for this reason, no SDE efficiency is obtained for this case. The analysis of energetics within the GL theory confirms that this helical spin-triplet pairing phase indeed stabilizes the LO state. Upon the application of a finite magnetic field, the LO phase is strongly suppressed and gives way to the corresponding zero-momentum SC state, while the chiral

spin-triplet p -wave state develops a finite Cooper-pair momentum with an FF modulation, whose SDE efficiency is quantitatively similar to the FF spin-singlet s -wave state counterpart. All technical details on the above analyses are explained in the SM [54].

Summary and outlook— In the present work, we have systematically studied the possible emergence of superconductivity with either zero or finite Cooper-pair center of mass momentum in recently proposed unconventional p -wave magnets from a GL theory perspective. Consequently, we have shown that, while for zero magnetic field a SC phase is obtained, an FF phase appears as the leading instability for a finite \mathbf{B} . By computing the efficiency of the SDE of the finite momentum pairing phase via the GL analysis, we have found that a high efficiency of the diode effect is expected in these systems for experimentally relevant UPM spin splittings. Therefore, our present results indicate that the experimental discovery of these new materials represents a promising platform for the design of energy-efficient logic circuits that can be ultimately used in the fields of classical and quantum computing, and in new superconducting sensors as well.

Since it has recently been demonstrated from a theoretical perspective that iron-based superconductors with coplanar magnetic order are likely odd-parity magnets [18, 19, 24], these compounds may provide a concrete materialization of odd-parity magnetism coexisting with superconductivity. In the specific case of the material LaFeAsO doped with phosphorus, coplanar magnetic order was experimentally shown to coexist with superconductivity within a particular region of the phase diagram [64]. Therefore, this compound represents to date the best candidate material for observing all the features investigated here, including a highly efficient SDE under the application of a magnetic field. For this reason, we hope that our present work can stimulate further experimental activities on the remarkable properties of such unconventional odd-parity magnetic compounds.

Acknowledgments— H.F. acknowledges funding from the Conselho Nacional de Desenvolvimento Científico e Tecnológico (CNPq) under Grant No. 404274/2023-4 and No. 305575/2025-2. We also acknowledge the support of the INCT project Advanced Quantum Materials, involving the Brazilian agencies CNPq (Proc. 408766/2024-7), FAPESP, and CAPES.

- [1] L. Šmejkal, J. Sinova, and T. Jungwirth, Beyond Conventional Ferromagnetism and Antiferromagnetism: A Phase with Nonrelativistic Spin and Crystal Rotation Symmetry, *Phys. Rev. X* **12**, 031042 (2022).
- [2] L. Šmejkal, J. Sinova, and T. Jungwirth, Emerging Research Landscape of Altermagnetism, *Phys. Rev. X* **12**, 040501 (2022).
- [3] I. Mazin (The PRX Editors), Editorial: Altermagnetism—a new punch line of fundamental magnetism, *Phys. Rev. X* **12**, 040002 (2022).
- [4] S. Hayami, Y. Yanagi, and H. Kusunose, Momentum-dependent spin splitting by collinear antiferromagnetic or

- dering, *Journal of the Physical Society of Japan* **88**, 123702 (2019).
- [5] J. Krempaský, L. Šmejkal, S. W. D’Souza, M. Hajlaoui, G. Springholz, K. Uhlířová, F. Alarab, P. C. Constanti-nou, V. Strokov, D. Usanov, W. R. Pudelko, R. González-Hernández, A. B. Hellenes, Z. Jansa, H. Reichlová, Z. Šobáň, R. D. G. Betancourt, P. Wadley, J. Sinova, D. Kriegner, J. Minár, J. H. Dil, and T. Jungwirth, Altermagnetic lifting of Kramers spin degeneracy, *Nature* **626**, 517 (2023).
- [6] S. Lee, S. Lee, S. Jung, J. Jung, D. Kim, Y. Lee, B. Seok, J. Kim, B. G. Park, L. Šmejkal, C.-J. Kang, and C. Kim, Broken Kramers Degeneracy in Altermagnetic MnTe, *Phys. Rev. Lett.* **132**, 036702 (2024).
- [7] T. Osumi, S. Souma, T. Aoyama, K. Yamauchi, A. Honma, K. Nakayama, T. Takahashi, K. Ohgushi, and T. Sato, Observation of a giant band splitting in altermagnetic MnTe, *Phys. Rev. B* **109**, 115102 (2024).
- [8] J. Ding, Z. Jiang, X. Chen, Z. Tao, Z. Liu, T. Li, J. Liu, J. Sun, J. Cheng, J. Liu, Y. Yang, R. Zhang, L. Deng, W. Jing, Y. Huang, Y. Shi, M. Ye, S. Qiao, Y. Wang, Y. Guo, D. Feng, and D. Shen, Large Band Splitting in g -Wave Altermagnet CrSb, *Phys. Rev. Lett.* **133**, 206401 (2024).
- [9] W. Lu, S. Feng, Y. Wang, D. Chen, Z. Lin, X. Liang, S. Liu, W. Feng, K. Yamagami, J. Liu, C. Felser, Q. Wu, and J. Ma, Signature of Topological Surface Bands in Altermagnetic Weyl Semimetal CrSb, *Nano Letters* **25**, 7343–7350 (2025).
- [10] C. Li, M. Hu, Z. Li, Y. Wang, W. Chen, B. Thiagarajan, M. Leandersson, C. Polley, T. Kim, H. Liu, C. Fulga, M. G. Vergniory, O. Janson, O. Tjernberg, and J. van den Brink, Topological Weyl altermagnetism in CrSb, *Communications Physics* **8**, 311 (2025).
- [11] R. González-Hernández, L. Šmejkal, K. Výborný, Y. Yaghagi, J. Sinova, T. c. v. Jungwirth, and J. Železný, Efficient electrical spin splitter based on nonrelativistic collinear antiferromagnetism, *Phys. Rev. Lett.* **126**, 127701 (2021).
- [12] S. Karube, T. Tanaka, D. Sugawara, N. Kadoguchi, M. Kohda, and J. Nitta, Observation of Spin-Splitter Torque in Collinear Antiferromagnetic RuO₂, *Phys. Rev. Lett.* **129**, 137201 (2022).
- [13] L. Šmejkal, A. B. Hellenes, R. González-Hernández, J. Sinova, and T. Jungwirth, Giant and tunneling magnetoresistance in unconventional collinear antiferromagnets with nonrelativistic spin-momentum coupling, *Phys. Rev. X* **12**, 011028 (2022).
- [14] A. Chakraborty, A. B. Hellenes, R. J.-U. Ubiergo, T. Jungwirth, L. Šmejkal, and J. Sinova, Highly efficient non-relativistic edelstein effect in nodal p -wave magnets, *Nature Communications* **16**, 7270 (2025).
- [15] A. B. Hellenes, T. Jungwirth, R. Jaeschke-Ubiergo, A. Chakraborty, J. Sinova, and L. Šmejkal, *P*-wave magnets (2024), arXiv:2309.01607 [cond-mat.mes-hall].
- [16] B. Brekke, P. Sukhachov, H. G. Giil, A. Brataas, and J. Linder, Minimal models and transport properties of unconventional p -wave magnets, *Phys. Rev. Lett.* **133**, 236703 (2024).
- [17] T. Jungwirth, R. M. Fernandes, E. Fradkin, A. H. MacDonald, J. Sinova, and L. Šmejkal, Altermagnetism: An unconventional spin-ordered phase of matter, *Newton* **1**, 100162 (2025).
- [18] Y. Yu, M. B. Lyngby, T. Shishidou, M. Roig, A. Kreisel, M. Weinert, B. M. Andersen, and D. F. Agterberg, Odd-parity magnetism driven by antiferromagnetic exchange, *Phys. Rev. Lett.* **135**, 046701 (2025).
- [19] C. Lee and P. M. R. Brydon, Inversion-asymmetric itinerant antiferromagnets by the space group symmetry, *Phys. Rev.*

Lett. **135**, 116701 (2025).

[20] M. Ezawa, Third-order and fifth-order nonlinear spin-current generation in *g*-wave and *i*-wave altermagnets and perfectly nonreciprocal spin current in *f*-wave magnets, *Phys. Rev. B* **111**, 125420 (2025).

[21] Y.-P. Lin, Odd-parity altermagnetism through sublattice currents: From Haldane-Hubbard model to general bipartite lattices (2025), arXiv:2503.09602 [cond-mat.str-el].

[22] M. Zeng, Z. Qin, L. Qin, S. Feng, D.-H. Xu, and R. Wang, The odd-parity altermagnetism: A spin group study (2025), arXiv:2507.09906 [cond-mat.str-el].

[23] Z.-Y. Zhuang, D. Zhu, D. Liu, Z. Wu, and Z. Yan, Odd-parity altermagnetism originated from orbital orders (2025), arXiv:2508.18361 [cond-mat.mes-hall].

[24] R. Dsouza, A. Kreisel, B. M. Andersen, D. F. Agterberg, and M. H. Christensen, Odd-Parity Magnetism in Fe-Based Superconductors (2025), arXiv:2508.21673 [cond-mat.supr-con].

[25] Q. Song, S. Stavrić, P. Barone, A. Droghetti, D. S. Antonenko, J. W. Venderbos, C. A. Occhialini, B. Ilyas, E. Ergeçen, N. Gedik, *et al.*, Electrical switching of a *p*-wave magnet, *Nature* **642**, 64 (2025).

[26] R. Yamada, M. T. Birch, P. R. Baral, S. Okumura, R. Nakano, S. Gao, M. Ezawa, T. Nomoto, J. Masell, Y. Ishihara, K. K. Kolincio, I. Belopolski, H. Sagayama, H. Nakao, K. Ohishi, T. Ohhara, R. Kiyanagi, T. Nakajima, Y. Tokura, T. hisa Arima, Y. Motome, M. M. Hirschmann, and M. Hirschberger, Metallic *p*-wave magnet with commensurate spin helix (2025), arXiv:2502.10386 [cond-mat.str-el].

[27] D. Zhu, Z.-Y. Zhuang, Z. Wu, and Z. Yan, Topological superconductivity in two-dimensional altermagnetic metals, *Phys. Rev. B* **108**, 184505 (2023).

[28] S. A. A. Ghorashi, T. L. Hughes, and J. Cano, Altermagnetic routes to majorana modes in zero net magnetization, *Phys. Rev. Lett.* **133**, 106601 (2024).

[29] Y.-X. Li and C.-C. Liu, Majorana corner modes and tunable patterns in an altermagnet heterostructure, *Phys. Rev. B* **108**, 205410 (2023).

[30] Y.-X. Li, Y. Liu, and C.-C. Liu, Creation and manipulation of higher-order topological states by altermagnets, *Phys. Rev. B* **109**, L201109 (2024).

[31] S.-B. Zhang, L.-H. Hu, and T. Neupert, Finite-momentum cooper pairing in proximitized altermagnets, *Nature Communications* **15**, 1801 (2024).

[32] D. Chakraborty and A. M. Black-Schaffer, Zero-field finite-momentum and field-induced superconductivity in altermagnets, *Phys. Rev. B* **110**, L060508 (2024).

[33] G. Sim and J. Knolle, Pair density waves and supercurrent diode effect in altermagnets, *Phys. Rev. B* **112**, L020502 (2025).

[34] S. Hong, M. J. Park, and K.-M. Kim, Unconventional *p*-wave and finite-momentum superconductivity induced by altermagnetism through the formation of Bogoliubov Fermi surface, *Phys. Rev. B* **111**, 054501 (2025).

[35] H. Hu, Z. Liu, and X.-J. Liu, Unconventional superconductivity of an altermagnetic metal: Polarized BCS and inhomogeneous FFLO states, *Phys. Rev. B* **112**, 184501 (2025).

[36] I. I. Mazin, Notes on altermagnetism and superconductivity (2022), arXiv:2203.05000 [cond-mat.supr-con].

[37] B. Brekke, A. Brataas, and A. Sudbø, Two-dimensional altermagnets: Superconductivity in a minimal microscopic model, *Phys. Rev. B* **108**, 224421 (2023).

[38] V. S. de Carvalho and H. Freire, Unconventional superconductivity in altermagnets with spin-orbit coupling, *Phys. Rev. B* **110**, L220503 (2024).

[39] D. Chakraborty and A. M. Black-Schaffer, Constraints on superconducting pairing in altermagnets, *Phys. Rev. B* **112**, 014516 (2025).

[40] K. Mukasa and Y. Masaki, Finite-momentum superconductivity in two-dimensional altermagnets with a rashba-type spin-orbit coupling, *Journal of the Physical Society of Japan* **94**, 064705 (2025).

[41] Y.-M. Wu, Y. Wang, and R. M. Fernandes, Intra-unit-cell singlet pairing mediated by altermagnetic fluctuations, *Phys. Rev. Lett.* **135**, 156001 (2025).

[42] N. Heinsdorf and M. Franz, Proximityalizing altermagnets with conventional superconductors (2025), arXiv:2509.03774 [cond-mat.supr-con].

[43] S. Ilić and F. S. Bergeret, Theory of the Supercurrent Diode Effect in Rashba Superconductors with Arbitrary Disorder, *Phys. Rev. Lett.* **128**, 177001 (2022).

[44] N. F. Q. Yuan and L. Fu, Supercurrent diode effect and finite-momentum superconductors, *Proceedings of the National Academy of Sciences* **119**, e2119548119 (2022).

[45] S. Banerjee and M. S. Scheurer, Altermagnetic superconducting diode effect, *Phys. Rev. B* **110**, 024503 (2024).

[46] D. Chakraborty and A. M. Black-Schaffer, Perfect superconducting diode effect in altermagnets, *Phys. Rev. Lett.* **135**, 026001 (2025).

[47] I. de M. Froldi and H. Freire, Efficiency of the superconducting diode effect of pair-density-wave states in two-dimensional *d*-wave altermagnets, *Annals of Physics* **483**, 170273 (2025).

[48] D. Shaffer and A. Levchenko, Theories of Superconducting Diode Effects (2025), arXiv:2510.25864 [cond-mat.supr-con].

[49] K. Maeda, Y. Fukaya, K. Yada, B. Lu, Y. Tanaka, and J. Cayao, Classification of pair symmetries in superconductors with unconventional magnetism, *Phys. Rev. B* **111**, 144508 (2025).

[50] Y. Fukaya, B. Lu, K. Yada, Y. Tanaka, and J. Cayao, Superconducting phenomena in systems with unconventional magnets, *Journal of Physics: Condensed Matter* **37**, 313003 (2025).

[51] Y. Nagae, L. Katayama, and S. Ikegaya, Flat-band zero-energy states and anomalous proximity effects in *p*-wave magnet-superconductor hybrid systems, *Phys. Rev. B* **111**, 174519 (2025).

[52] P. Sukhachov, H. G. Giil, B. Brekke, and J. Linder, Coexistence of *p*-wave magnetism and superconductivity, *Phys. Rev. B* **111**, L220403 (2025).

[53] T. Kokkeler, I. Tokatly, and F. S. Bergeret, Quantum transport theory for unconventional magnets: Interplay of altermagnetism and *p*-wave magnetism with superconductivity, *SciPost Phys.* **18**, 178 (2025).

[54] See Supplemental Material at [URL will be inserted by publisher] for further information on the derivation of the superconducting gap equations, the calculation of the coefficients of the Ginzburg-Landau free energy, and the detailed analysis of the emergence of superconductivity and PDW in both spin-singlet and spin-triplet channels.

[55] R. Soto-Garrido and E. Fradkin, Pair-density-wave superconducting states and electronic liquid-crystal phases, *Phys. Rev. B* **89**, 165126 (2014).

[56] P. Fulde and R. A. Ferrell, Superconductivity in a strong spin-exchange field, *Phys. Rev.* **135**, A550 (1964).

[57] D. F. Agterberg, J. S. Davis, S. D. Edkins, E. Fradkin, D. J. Van Harlingen, S. A. Kivelson, P. A. Lee, L. Radzihovsky, J. M. Tranquada, and Y. Wang, The physics of pair-density waves: Cuprate superconductors and beyond, *Annual Review of Condensed Matter Physics* **11**, 231 (2020).

[58] P. A. Frigeri, D. F. Agterberg, A. Koga, and M. Sigrist, Superconductivity without Inversion Symmetry: MnSi versus

CePt₃Si, *Phys. Rev. Lett.* **92**, 097001 (2004).

[59] L. S. Levitov, Y. V. Nazarov, and G. M. Eliashberg, Magnetostatics of superconductors without an inversion center, *JETP Lett.* **41**, 9 (1985).

[60] V. M. Edelstein, The Ginzburg-Landau equation for superconductors of polar symmetry, *Journal of Physics: Condensed Matter* **8**, 339 (1996).

[61] F. Ando, Y. Miyasaka, T. Li, J. Ishizuka, T. Arakawa, Y. Shiota, T. Moriyama, Y. Yanase, and T. Ono, Observation of superconducting diode effect, *Nature* **584**, 373 (2020).

[62] B. A. Bernevig and T. L. Hughes, *Topological Insulators and Topological Superconductors* (Princeton University Press, Princeton, 2013).

[63] A. I. Larkin and Y. N. Ovchinnikov, Nonuniform state of superconductors, *Sov. Phys. JETP* **20**, 762 (1965).

[64] R. Stadel, D. D. Khalyavin, P. Manuel, K. Yokoyama, S. Lapidus, M. H. Christensen, R. M. Fernandes, D. Phelan, D. Y. Chung, R. Osborn, *et al.*, Multiple magnetic orders in LaFeAs_{1-x}P_xO uncover universality of iron-pnictide superconductors, *Communications Physics* **5**, 146 (2022).

Supplemental Material:
Highly efficient superconducting diode effect in unconventional p -wave magnets

Igor de M. Froldi and Hermann Freire

Instituto de Física, Universidade Federal de Goiás, 74.690-900, Goiânia-GO, Brazil

In this Supplemental Material, we extend the analysis and also give detailed derivations of the results discussed in the main text.

THE EFFECTIVE MODEL

The effective model for the unconventional p -wave magnet (UPM) given in the main text has the noninteracting Hamiltonian given by:

$$H_0 = \sum_{\mathbf{k}, s, s'} \psi_{\mathbf{k}, s}^\dagger [\mathbb{1} \xi_{\mathbf{k}} + \lambda \mathbf{g}_{\mathbf{k}} \cdot \boldsymbol{\sigma} + \mathbf{B} \cdot \boldsymbol{\sigma}]_{s, s'} \psi_{\mathbf{k}, s'} \equiv \sum_{\mathbf{k}} \mathcal{H}_0(\mathbf{k}), \quad (\text{S1})$$

where the energy dispersion is $\xi_{\mathbf{k}} = \mathbf{k}^2/(2m) - \mu$. This Hamiltonian describes a UPM (we assume that $\mathbf{g}_{\mathbf{k}} = k_x \hat{\mathbf{z}}$ in the vicinity of the Γ point) parametrized by the spin-splitting strength λ . We also define the effective coupling $\mathbf{g}_{\mathbf{k}}^{\text{eff}} = \lambda \mathbf{g}_{\mathbf{k}} + \mathbf{B}$. The superconducting instabilities are studied by adding a BCS-type attractive interaction given by:

$$H_{\text{int}} = \frac{1}{2} \sum_{\mathbf{k}, s, s'} V_{\mathbf{k}, \mathbf{k}'} \psi_{\mathbf{k}+\mathbf{q}/2, s}^\dagger \psi_{-\mathbf{k}+\mathbf{q}/2, s'}^\dagger \psi_{-\mathbf{k}'+\mathbf{q}/2, s'} \psi_{\mathbf{k}'+\mathbf{q}/2, s}, \quad (\text{S2})$$

where $V_{\mathbf{k}, \mathbf{k}'} < 0$ and we have taken the volume of the system to be equal to unity. We decouple the above interaction in the pairing channel by defining the pairing function $\widehat{\mathcal{F}}_{\mathbf{Q}}(\mathbf{k})$:

$$\langle \psi_{-\mathbf{k}+\mathbf{q}/2, s'} \psi_{\mathbf{k}+\mathbf{q}/2, s} \rangle \equiv \sum_{\{\mathbf{Q}\}} \delta_{\mathbf{q}, \mathbf{Q}} \left[\widehat{\mathcal{F}}_{\mathbf{Q}}(\mathbf{k}) i\sigma_y \right]_{s, s'}, \quad (\text{S3})$$

and the sum in \mathbf{Q} is discrete over some particular values (to be determined later). We define the order parameter field $\widehat{\Delta}_{\mathbf{Q}}(\mathbf{k})$ as:

$$\widehat{\Delta}_{\mathbf{Q}}(\mathbf{k}) \equiv - \sum_{\mathbf{k}'} V_{\mathbf{k}, \mathbf{k}'} \widehat{\mathcal{F}}_{\mathbf{Q}}(\mathbf{k}) \Rightarrow \widehat{\mathcal{F}}_{\mathbf{Q}}(\mathbf{k}) = - \sum_{\mathbf{k}'} V_{\mathbf{k}', \mathbf{k}}^{-1} \widehat{\Delta}_{\mathbf{Q}}(\mathbf{k}). \quad (\text{S4})$$

Using the Nambu basis $\Psi_{\mathbf{k}} = (\psi_{\mathbf{k}, \uparrow} \quad \psi_{\mathbf{k}, \downarrow} \quad \psi_{-\mathbf{k}, \uparrow}^\dagger \quad \psi_{-\mathbf{k}, \downarrow}^\dagger)^T$, we write the full Hamiltonian $H = H_0 + H_{\text{int}}$ as:

$$H = \frac{1}{2} \sum_{\mathbf{k}, \mathbf{k}'} \Psi_{\mathbf{k}'}^\dagger \begin{pmatrix} \mathcal{H}_0(\mathbf{k}) \delta_{\mathbf{k}, \mathbf{k}'} & \Delta(\mathbf{k}, \mathbf{k}', \mathbf{Q}) \\ [\Delta(\mathbf{k}', \mathbf{k}, \mathbf{Q})]^\dagger & -[\mathcal{H}_0(\mathbf{k})]^T \delta_{\mathbf{k}, \mathbf{k}'} \end{pmatrix} \Psi_{\mathbf{k}} + \frac{1}{2} \sum_{\mathbf{k}, \{\mathbf{Q}\}} \text{tr} \left(\left[\widehat{\mathcal{F}}_{\mathbf{Q}}(\mathbf{k}) \right]^\dagger \widehat{\Delta}_{\mathbf{Q}}(\mathbf{k}) \right), \quad (\text{S5})$$

where:

$$\Delta(\mathbf{k}, \mathbf{k}', \mathbf{Q}) = \sum_{\{\mathbf{Q}\}} \widehat{\Delta}_{\mathbf{Q}} \left(\frac{\mathbf{k} + \mathbf{k}'}{2} \right) i\sigma_y \delta_{\mathbf{k}, \mathbf{k}' + \mathbf{Q}}. \quad (\text{S6})$$

The microscopic action is then obtained by $\mathcal{S}[\bar{\psi}, \psi, \bar{\Delta}, \Delta] = \int_0^\beta d\tau \left(\frac{1}{2} \Psi^\dagger \partial_\tau \Psi + H \right)$, where $\beta = 1/T$ is the inverse temperature. In Matsubara frequency space, we get for the microscopic action:

$$\begin{aligned} \mathcal{S} &= \frac{1}{2} T \sum_{\mathbf{k}, \mathbf{k}', i\omega_n} \Psi_{\mathbf{k}'}^\dagger \begin{pmatrix} [-i\omega_n + \mathcal{H}_0(\mathbf{k})] \delta_{\mathbf{k}, \mathbf{k}'} & \Delta(\mathbf{k}, \mathbf{k}', \mathbf{Q}) \\ [\Delta(\mathbf{k}', \mathbf{k}, \mathbf{Q})]^\dagger & [-i\omega_n - [\mathcal{H}_0(\mathbf{k})]^T] \delta_{\mathbf{k}, \mathbf{k}'} \end{pmatrix} \Psi_{\mathbf{k}} + \frac{\beta}{2} \sum_{\mathbf{k}, \{\mathbf{Q}\}} \text{tr} \left(\left[\widehat{\mathcal{F}}_{\mathbf{Q}}(\mathbf{k}) \right]^\dagger \widehat{\Delta}_{\mathbf{Q}}(\mathbf{k}) \right) \\ &\equiv \frac{1}{2} T \sum_{\mathbf{k}, \mathbf{k}', i\omega_n} \Psi_{\mathbf{k}'}^\dagger \left(\left[\widehat{\mathcal{G}}_0(\mathbf{k}, i\omega_n) \right]^{-1} \delta_{\mathbf{k}, \mathbf{k}'} + \widehat{\mathcal{M}}(\mathbf{k}, \mathbf{k}', \mathbf{Q}) \right) \Psi_{\mathbf{k}} + \frac{\beta}{2} \sum_{\mathbf{k}, \{\mathbf{Q}\}} \text{tr} \left(\left[\widehat{\mathcal{F}}_{\mathbf{Q}}(\mathbf{k}) \right]^\dagger \widehat{\Delta}_{\mathbf{Q}}(\mathbf{k}) \right), \end{aligned} \quad (\text{S7})$$

where a constant term was dropped since it represents only a shift in total energy. Also, we defined the inverse of the free propagator $\widehat{\mathcal{G}}_0(\mathbf{k}, i\omega_n)$ (with $\omega_n = (2n+1)\pi T, n \in \mathbb{N}$) and the order-parameter matrix is given by $\widehat{\mathcal{M}}(\mathbf{k}, \mathbf{k}', \mathbf{Q})$. Written in terms of the particle and hole propagators, the inverse of the free propagator becomes:

$$\left[\widehat{\mathcal{G}}_0(\mathbf{k}, i\omega_n) \right]^{-1} \equiv \begin{pmatrix} [-i\omega_n + \mathcal{H}_0(\mathbf{k})] \delta_{\mathbf{k}, \mathbf{k}'} & 0 \\ 0 & [-i\omega_n - [\mathcal{H}_0(\mathbf{k})]^T] \delta_{\mathbf{k}, \mathbf{k}'} \end{pmatrix} = \begin{pmatrix} \left[G_0^{(p)}(\mathbf{k}, i\omega_n) \right]^{-1} & 0 \\ 0 & \left[G_0^{(h)}(\mathbf{k}, i\omega_n) \right]^{-1} \end{pmatrix}, \quad (\text{S8})$$

where:

$$G_0^{(p)}(\mathbf{k}, i\omega_n) = \frac{1}{(-i\omega_n + \xi_{\mathbf{k}}) \sigma_0 + \mathbf{g}_{\mathbf{k}}^{\text{eff}} \cdot \boldsymbol{\sigma}}, \quad (\text{S9})$$

$$G_0^{(h)}(\mathbf{k}, i\omega_n) = \frac{1}{(-i\omega_n - \xi_{-\mathbf{k}}) \sigma_0 + \mathbf{g}_{-\mathbf{k}}^{\text{eff}} \cdot \sigma_y \boldsymbol{\sigma} \sigma_y} \quad (\text{S10})$$

can be further simplified to:

$$G_0^{(p)}(\mathbf{k}, i\omega_n) = G^{(+)}(\mathbf{k}, i\omega_n) \sigma_0 + G^{(-)}(\mathbf{k}, i\omega_n) \widehat{\mathbf{g}}_{\mathbf{k}}^{\text{eff}} \cdot \boldsymbol{\sigma}, \quad (\text{S11})$$

$$G_0^{(h)}(\mathbf{k}, i\omega_n) = -G^{(+)}(-\mathbf{k}, -i\omega_n) \sigma_0 + G^{(-)}(-\mathbf{k}, -i\omega_n) \widehat{\mathbf{g}}_{-\mathbf{k}}^{\text{eff}} \cdot \sigma_y \boldsymbol{\sigma} \sigma_y, \quad (\text{S12})$$

(where $\widehat{\mathbf{g}}_{\mathbf{k}}^{\text{eff}} \equiv \mathbf{g}_{\mathbf{k}}^{\text{eff}} / |\mathbf{g}_{\mathbf{k}}^{\text{eff}}|$) by defining:

$$G^{(+)}(\mathbf{k}, i\omega_n) = \frac{1}{2} \left(\frac{1}{-i\omega_n + \xi_{\mathbf{k}} + |\mathbf{g}_{\mathbf{k}}^{\text{eff}}|} + \frac{1}{-i\omega_n + \xi_{\mathbf{k}} - |\mathbf{g}_{\mathbf{k}}^{\text{eff}}|} \right),$$

$$G^{(-)}(\mathbf{k}, i\omega_n) = \frac{1}{2} \left(\frac{1}{-i\omega_n + \xi_{\mathbf{k}} + |\mathbf{g}_{\mathbf{k}}^{\text{eff}}|} - \frac{1}{-i\omega_n + \xi_{\mathbf{k}} - |\mathbf{g}_{\mathbf{k}}^{\text{eff}}|} \right).$$

We now work out the last term in Eq. (S7). As explained in the main text, in order to present a complete picture of possible SC phases emerging from a UPM, we decompose the pairing order parameter matrix as:

$$\widehat{\Delta}^{(\mathbf{q})}(\mathbf{k}) = \Delta_s^{(\mathbf{q})}(\mathbf{k}) \sigma_0 + \Delta_t^{(\mathbf{q})}(\mathbf{k}) \cdot \boldsymbol{\sigma}, \quad (\text{S13})$$

where $\Delta_s^{(\mathbf{q})}(\mathbf{k})$ and $\Delta_t^{(\mathbf{q})}(\mathbf{k})$ refer to the singlet and triplet pairing amplitudes, respectively. We take $\Delta_s^{(\mathbf{q})}(\mathbf{k})$ and $\Delta_t^{(\mathbf{q})}(\mathbf{k})$ to obey:

$$\sum_{\mathbf{k}'} V_{\mathbf{k}, \mathbf{k}'} \Delta_s^{(\mathbf{q})}(\mathbf{k}') \equiv -V_s \Delta_s^{(\mathbf{q})}(\mathbf{k}), \quad (\text{S14})$$

$$\sum_{\mathbf{k}'} V_{\mathbf{k}, \mathbf{k}'} \Delta_t^{(\mathbf{q})}(\mathbf{k}') \equiv -V_t \Delta_t^{(\mathbf{q})}(\mathbf{k}), \quad (\text{S15})$$

with $V_s > 0$ and $V_t > 0$ referring to the pair couplings in the singlet and triplet channels, respectively. The minus sign in the r.h.s. of Eqs. (S14) and (S15) comes from the attractive character of the interactions near the Fermi surface. Consequently, the last term in Eq. (S7) becomes after some algebra:

$$I = \frac{1}{2} \text{tr} \left(\left[\widehat{\mathcal{F}}_{\mathbf{Q}}(\mathbf{k}) \right]^{\dagger} \widehat{\Delta}_{\mathbf{Q}}(\mathbf{k}) \right) = \sum_{\mathbf{p}, \{\mathbf{Q}\}} \left(\frac{1}{V_s} |\Delta_s^{(\mathbf{Q})}(\mathbf{p})|^2 + \frac{1}{V_t} |\Delta_t^{(\mathbf{Q})}(\mathbf{p})|^2 \right).$$

We write the singlet and triplet pairing order parameters as:

$$\Delta_s^{(\mathbf{q})}(\mathbf{k}) = \Delta_s^{(\mathbf{q})} d_0(\mathbf{k}), \quad (\text{S16})$$

$$\Delta_t^{(\mathbf{q})}(\mathbf{k}) = \Delta_t^{(\mathbf{q})} \mathbf{d}(\mathbf{k}), \quad (\text{S17})$$

where $\Delta_s^{(\mathbf{q})} = |\Delta_s^{(\mathbf{q})}| e^{i\theta_s}$ and $\Delta_t^{(\mathbf{q})} = |\Delta_t^{(\mathbf{q})}| e^{i\theta_t}$, with θ_s and θ_t being, respectively, the phases of the order parameter field in the singlet and triplet channels. As required by Fermi-Dirac statistics, $d_0(\mathbf{k}) = d_0(-\mathbf{k})$ and $\mathbf{d}(\mathbf{k}) = -\mathbf{d}(-\mathbf{k})$. We also take the form factors $d_0(\mathbf{k})$ and $\mathbf{d}(\mathbf{k})$ to be normalized over the Fermi surface, i.e.

$$\int_{FS} \frac{d\theta}{2\pi} |d_0(\mathbf{k})|^2 = 1, \quad (\text{S18})$$

$$\int_{FS} \frac{d\theta}{2\pi} |\mathbf{d}(\mathbf{k})|^2 = 1. \quad (\text{S19})$$

Then, we obtain:

$$I = \frac{1}{V_s} \sum_{\{\mathbf{Q}\}} |\Delta_s^{(\mathbf{Q})}|^2 + \frac{1}{V_t} \sum_{\{\mathbf{Q}\}} |\Delta_t^{(\mathbf{Q})}|^2.$$

Now, we are able to write the full microscopic action as:

$$\mathcal{S} = \frac{1}{2\beta} \sum_{\mathbf{k}, \mathbf{k}', i\omega_n} \Psi_{\mathbf{k}'}^\dagger \left(\left[\hat{\mathcal{G}}_0(\mathbf{k}, i\omega_n) \right]^{-1} \delta_{\mathbf{k}, \mathbf{k}'} + \hat{\mathcal{M}}(\mathbf{k}, \mathbf{k}', \{\mathbf{Q}\}) \right) \Psi_{\mathbf{k}} + \beta \sum_{\{\mathbf{Q}\}} \left(\frac{1}{V_s} |\Delta_s^{(\mathbf{Q})}|^2 + \frac{1}{V_t} |\Delta_t^{(\mathbf{Q})}|^2 \right).$$

GINZBURG-LANDAU EXPANSION

The partition function of the effective model can be calculated using the path integral formalism. Integrating out the fermionic fields Ψ^\dagger, Ψ , we get:

$$\mathcal{Z} [\Delta^\dagger, \Delta] = \int \mathcal{D}[\Psi^\dagger, \Psi] e^{-\mathcal{S}[\Psi^\dagger, \Psi]} = \det \left(\left[\hat{\mathcal{G}}_0 \right]^{-1} + \hat{\mathcal{M}} \right) \exp \left[\frac{\beta}{2} \sum_{\{\mathbf{Q}\}} \left(\frac{1}{V_s} |\Delta_s^{(\mathbf{Q})}|^2 + \frac{1}{V_t} |\Delta_t^{(\mathbf{Q})}|^2 \right) \right]. \quad (\text{S20})$$

Since $\mathcal{Z} [\Delta^\dagger, \Delta] = e^{-\beta \mathcal{F} [\Delta^\dagger, \Delta]}$, where $\mathcal{F} [\Delta^\dagger, \Delta]$ is the free energy for the order parameter field. Using $\det(A) = e^{\text{Tr}\{\ln(A)\}}$, we get the Ginzburg-Landau (GL) free energy:

$$\mathcal{F} [\Delta^\dagger, \Delta] = -\frac{1}{\beta} \text{Tr}\{\mathcal{G}_0^{-1}\} + \frac{1}{\beta} \sum_{n=1}^{\infty} \frac{1}{2n} \text{Tr} \left\{ \left(\hat{\mathcal{G}}_0 \hat{\mathcal{M}} \right)^{2n} \right\} - \frac{1}{2} \sum_{\{\mathbf{Q}\}} \left(\frac{1}{V_s} |\Delta_s^{(\mathbf{Q})}|^2 + \frac{1}{V_t} |\Delta_t^{(\mathbf{Q})}|^2 \right), \quad (\text{S21})$$

where Tr stands for $\sum_{\mathbf{k}, i\omega_n} \text{tr}$, and tr refers to the trace over spin indices, and $\mathcal{F}_0 = -\frac{1}{\beta} \text{Tr}\{\mathcal{G}_0^{-1}\}$ is the free energy of the normal phase, which we disregard from now on. Each of the term of order $2n$ in the sum above describes a one-particle irreducible diagram with $2n$ insertions of the complex fields Δ or Δ^\dagger . The second-order coefficient of GL expansion describes a “mass” term which will encode the linearized gap equation, the identification of the transition temperature and the Cooper pair momentum \mathbf{Q} that minimizes the GL free energy. If $\mathbf{Q} = 0$, one recovers a traditional zero-momentum SC phase, while if \mathbf{Q} is finite, one obtains a PDW state (which can be either an FF phase or an LO phase – to be explained in more detail below). The fourth-order term of Eq. (S21) describes the stability of the corresponding phase w.r.t. the interactions. In order for the GL free energy to be bounded from below, the coefficient of this fourth-order term must be positive.

Using the definitions of the order parameter field, Eq. (S6), and the definitions of the particle and hole propagators, Eqs. (S11) and (S12), the second-order part of the free energy \mathcal{F}_2 is given by [using the notation $G^{(\pm)}(\mathbf{k} + \frac{\mathbf{q}}{2}) \equiv G^{(\pm)}$ and $G^{(\pm)}(-\mathbf{k} + \frac{\mathbf{q}}{2}) \equiv \tilde{G}^{(\pm)}$]:

$$\mathcal{F}_2 [\Delta^\dagger, \Delta] = \sum_{\{\mathbf{Q}\}} \left(\alpha_s(\mathbf{Q}, T) |\Delta_s^{(\mathbf{Q})}|^2 + \alpha_t(\mathbf{Q}, T) |\Delta_t^{(\mathbf{Q})}|^2 + \alpha_{st}(\mathbf{Q}, T) |\Delta_s^{(\mathbf{Q})}| |\Delta_t^{(\mathbf{Q})}| \right), \quad (\text{S22})$$

where:

$$\alpha_s(\mathbf{q}, T) = \frac{1}{V_s} + 2T \sum_{\mathbf{k}, i\omega_n} d_0^2(\mathbf{k}) \left(-G^{(+)} \tilde{G}^{(+)} + G^{(-)} \tilde{G}^{(-)} \hat{\mathbf{g}}_{\mathbf{k}+\frac{\mathbf{q}}{2}}^{\text{eff}} \cdot \hat{\mathbf{g}}_{-\mathbf{k}+\frac{\mathbf{q}}{2}}^{\text{eff}} \right), \quad (\text{S23})$$

$$\begin{aligned} \alpha_t(\mathbf{q}, T) = & \frac{1}{V_t} + 2T \sum_{\mathbf{k}, i\omega_n} \left(|\mathbf{d}(\mathbf{k})|^2 \left\{ -G^{(+)} \tilde{G}^{(+)} - G^{(-)} \tilde{G}^{(-)} \hat{\mathbf{g}}_{\mathbf{k}+\frac{\mathbf{q}}{2}}^{\text{eff}} \cdot \hat{\mathbf{g}}_{-\mathbf{k}+\frac{\mathbf{q}}{2}}^{\text{eff}} \right\} \right. \\ & \left. + 2 \left[\mathbf{d}(\mathbf{k}) \cdot \hat{\mathbf{g}}_{\mathbf{k}+\frac{\mathbf{q}}{2}}^{\text{eff}} \right] \left[\mathbf{d}^*(\mathbf{k}) \cdot \hat{\mathbf{g}}_{-\mathbf{k}+\frac{\mathbf{q}}{2}}^{\text{eff}} \right] G^{(-)} \tilde{G}^{(-)} \right), \end{aligned} \quad (\text{S24})$$

$$\alpha_{st}(\mathbf{q}, T) = -4T \sum_{\mathbf{k}, i\omega_n} d_0(\mathbf{k}) \left[\hat{\mathbf{g}}_{\mathbf{k}+\frac{\mathbf{q}}{2}}^{\text{eff}} \times \hat{\mathbf{g}}_{-\mathbf{k}+\frac{\mathbf{q}}{2}}^{\text{eff}} \right] \cdot \text{Im} \left\{ \mathbf{d}(\mathbf{k}) e^{i(\theta_s - \theta_t)} \right\} G^{(-)} \tilde{G}^{(-)}. \quad (\text{S25})$$

The linearized gap equations can be obtained from Eq. (S22) by the minimization of the singlet and triplet order parameter fields. Note that the term $\alpha_{st}(\mathbf{q}, T)$ couples both the singlet and the triplet equations in general. However, for the cases investigated in this work, since $\hat{\mathbf{g}}_{\mathbf{k}}^{\text{eff}} \sim \hat{\mathbf{z}}$, this leads to $\alpha_{st}(\mathbf{q}, T) = 0$ for all temperatures and momenta. Then, the linearized equations for the spin-singlet critical temperature $T_c^{(s)}$ and spin-triplet critical temperature $T_c^{(t)}$ are, respectively, given by $\alpha_s(\mathbf{Q}, T_c^{(s)}) = 0$ and $\alpha_t(\mathbf{Q}, T_c^{(t)}) = 0$, where \mathbf{Q} is the previously mentioned minimizing wave vector.

Next, we evaluate the sums and integrals of the coefficients $\alpha_s(\mathbf{q}, T)$ and $\alpha_t(\mathbf{q}, T)$ in Eqs. (S23) and (S24). To this end, we follow the usual BCS procedure by considering that the interactions promoting the SC instability are in the vicinity of the Fermi surface within a range given by $-\epsilon_c < \xi_{\mathbf{k}} < \epsilon_c$. Using the fact that this cutoff is the largest energy scale of the problem, we only retain the cutoff-dependent terms and absorb them by defining the singlet and triplet critical temperatures in the absence of UPM spin splitting λ and magnetic field \mathbf{B} (i.e., $\mathbf{g}_{\mathbf{k}}^{\text{eff}} = 0$), respectively, by:

$$T_{c,0}^{(s)} = \frac{2e^{\gamma}\epsilon_c}{\pi} e^{-1/N_F V_s}, \quad (\text{S26})$$

$$T_{c,0}^{(t)} = \frac{2e^{\gamma}\epsilon_c}{\pi} e^{-1/N_F V_t}, \quad (\text{S27})$$

where $\gamma = 0.57721\dots$ is the Euler-Mascheroni constant. Using the digamma function $\psi^{(0)}(x)$ to define $\Xi(x) = \text{Re}[\psi^{(0)}(\frac{1}{2} + ix)] - \psi^{(0)}(\frac{1}{2})$, the second-order coefficients in the GL expansion become:

$$\begin{aligned} \alpha_s(\mathbf{q}, T) = & N_F \ln \left(\frac{T}{T_{c,s}^{(0)}} \right) + \frac{N_F}{4} \sum_{\gamma=\pm} \int_{FS} \frac{d\theta}{2\pi} d_0^2(\mathbf{k}) \\ & \left(\Xi \left(\frac{\gamma g_1 + \frac{\mathbf{q}}{2} \cdot \mathbf{v}_F}{2\pi T} \right) \left(1 + \hat{\mathbf{g}}_{\mathbf{k}+\frac{\mathbf{q}}{2}}^{\text{eff}} \cdot \hat{\mathbf{g}}_{-\mathbf{k}+\frac{\mathbf{q}}{2}}^{\text{eff}} \right) + \Xi \left(\frac{\gamma g_2 + \frac{\mathbf{q}}{2} \cdot \mathbf{v}_F}{2\pi T} \right) \left(1 - \hat{\mathbf{g}}_{\mathbf{k}+\frac{\mathbf{q}}{2}}^{\text{eff}} \cdot \hat{\mathbf{g}}_{-\mathbf{k}+\frac{\mathbf{q}}{2}}^{\text{eff}} \right) \right), \end{aligned} \quad (\text{S28})$$

$$\begin{aligned} \alpha_t(\mathbf{q}, T) = & N_F \ln \left(\frac{T}{T_{c,t}^{(0)}} \right) + \frac{N_F}{4} \sum_{\gamma=\pm} \int_{FS} \frac{d\theta}{2\pi} \\ & \left(|\mathbf{d}(\mathbf{k})|^2 \left[\Xi \left(\frac{\gamma g_1 + \frac{\mathbf{q}}{2} \cdot \mathbf{v}_F}{2\pi T} \right) \left(1 - \hat{\mathbf{g}}_{\mathbf{k}+\frac{\mathbf{q}}{2}}^{\text{eff}} \cdot \hat{\mathbf{g}}_{-\mathbf{k}+\frac{\mathbf{q}}{2}}^{\text{eff}} \right) + \Xi \left(\frac{\gamma g_2 + \frac{\mathbf{q}}{2} \cdot \mathbf{v}_F}{2\pi T} \right) \left(1 + \hat{\mathbf{g}}_{\mathbf{k}+\frac{\mathbf{q}}{2}}^{\text{eff}} \cdot \hat{\mathbf{g}}_{-\mathbf{k}+\frac{\mathbf{q}}{2}}^{\text{eff}} \right) \right] \right. \\ & \left. + 2 \left[\mathbf{d}(\mathbf{k}) \cdot \hat{\mathbf{g}}_{\mathbf{k}+\frac{\mathbf{q}}{2}}^{\text{eff}} \right] \left[\mathbf{d}(\mathbf{k}) \cdot \hat{\mathbf{g}}_{-\mathbf{k}+\frac{\mathbf{q}}{2}}^{\text{eff}} \right] \left[\Xi \left(\frac{\gamma g_1 + \frac{\mathbf{q}}{2} \cdot \mathbf{v}_F}{2\pi T} \right) - \Xi \left(\frac{\gamma g_2 + \frac{\mathbf{q}}{2} \cdot \mathbf{v}_F}{2\pi T} \right) \right] \right). \end{aligned} \quad (\text{S29})$$

In Eqs. (S28) and (S29), $g_{1,2} = (|\mathbf{g}_{\mathbf{k}+\frac{\mathbf{q}}{2}}^{\text{eff}}| \pm |\mathbf{g}_{-\mathbf{k}+\frac{\mathbf{q}}{2}}^{\text{eff}}|)/2$ and $\mathbf{v}_F = k_F(\cos\theta\hat{\mathbf{x}} + \sin\theta\hat{\mathbf{y}})/m$ is the Fermi velocity at the Fermi level.

The plot of the coefficients (S28) and (S29) reveals the possible minimization wave vectors at a given temperature. For this reason, we show in Figs. S1(a), S1(b), S1(c) and S1(d), respectively, the cases for singlet *s*-wave and *d*-wave pairing states for both zero and finite magnetic field at a fixed temperature, revealing the emergence of a single minimum in the corresponding second-order GL coefficient. In Fig. S1(e), we show the triplet *p*-wave equal-spin (i.e., the helical-type) with gap function $\mathbf{d}(\mathbf{k}) = i(k_x\hat{\mathbf{y}} + k_y\hat{\mathbf{x}})$ for zero magnetic field. The triplet *p*-wave mixed-spin (i.e., the chiral-type) with gap function $\mathbf{d}(\mathbf{k}) = (k_x + ik_y)\hat{\mathbf{z}}$ yields a similar plot to those for singlet *s*-wave states.

In order to determine the critical temperature of each phase, we numerically minimize the coefficients α_s and α_t with respect to the external momentum \mathbf{q} , thus obtaining the temperature profile of the minimization wave vector as a function of temperature, $\mathbf{Q}(T)$. Then, we calculate the critical temperatures via the linearized gap equations:

$$\alpha_s \left(\mathbf{Q}(T_c^{(s)}), T_c^{(s)} \right) = 0, \quad (\text{S30})$$

$$\alpha_t \left(\mathbf{Q}(T_c^{(t)}), T_c^{(t)} \right) = 0. \quad (\text{S31})$$

Since we have shown that our model only displays one minimization wave vector for singlet states (\mathbf{Q}) and at most two finite minimization wave vectors for triplet states ($\pm\mathbf{Q}$), the possible PDW phases and their spatial modulations present in the effective model investigated here are:

a) *Fulde-Ferrell* (FF) *phase*: This pairing phase selects only one finite wave vector, thereby breaking spontaneously both time-reversal and inversion symmetries. This phase can emerge both for singlet and triplet states in the present model, and the real space modulation of the corresponding order parameter is given by:

$$\Delta_s^{\text{FF}}(\mathbf{r}) = \Delta_s^{(\mathbf{Q})} e^{i\mathbf{Q}\cdot\mathbf{r}} \quad (\text{singlet FF states}), \quad (\text{S32})$$

$$\Delta_t^{\text{FF}}(\mathbf{r}) = \Delta_t^{(\mathbf{Q})} e^{i\mathbf{Q}\cdot\mathbf{r}} \quad (\text{triplet FF states}). \quad (\text{S33})$$

b) *Larkin-Ovchinnikov* (LO) *phase*: This pairing phase is characterized by the two finite momenta, $\pm\mathbf{Q}$. Therefore, this is a time-reversal and inversion invariant version of the FF phase. This phase can only emerge for triplet states in the present model, and the real space modulation of the order parameter corresponding to this phase is:

$$\Delta_t^{\text{LO}}(\mathbf{r}) = \Delta_t^{(\mathbf{Q})} e^{i\mathbf{Q}\cdot\mathbf{r}} + \Delta_t^{(-\mathbf{Q})} e^{-i\mathbf{Q}\cdot\mathbf{r}}. \quad (\text{S34})$$

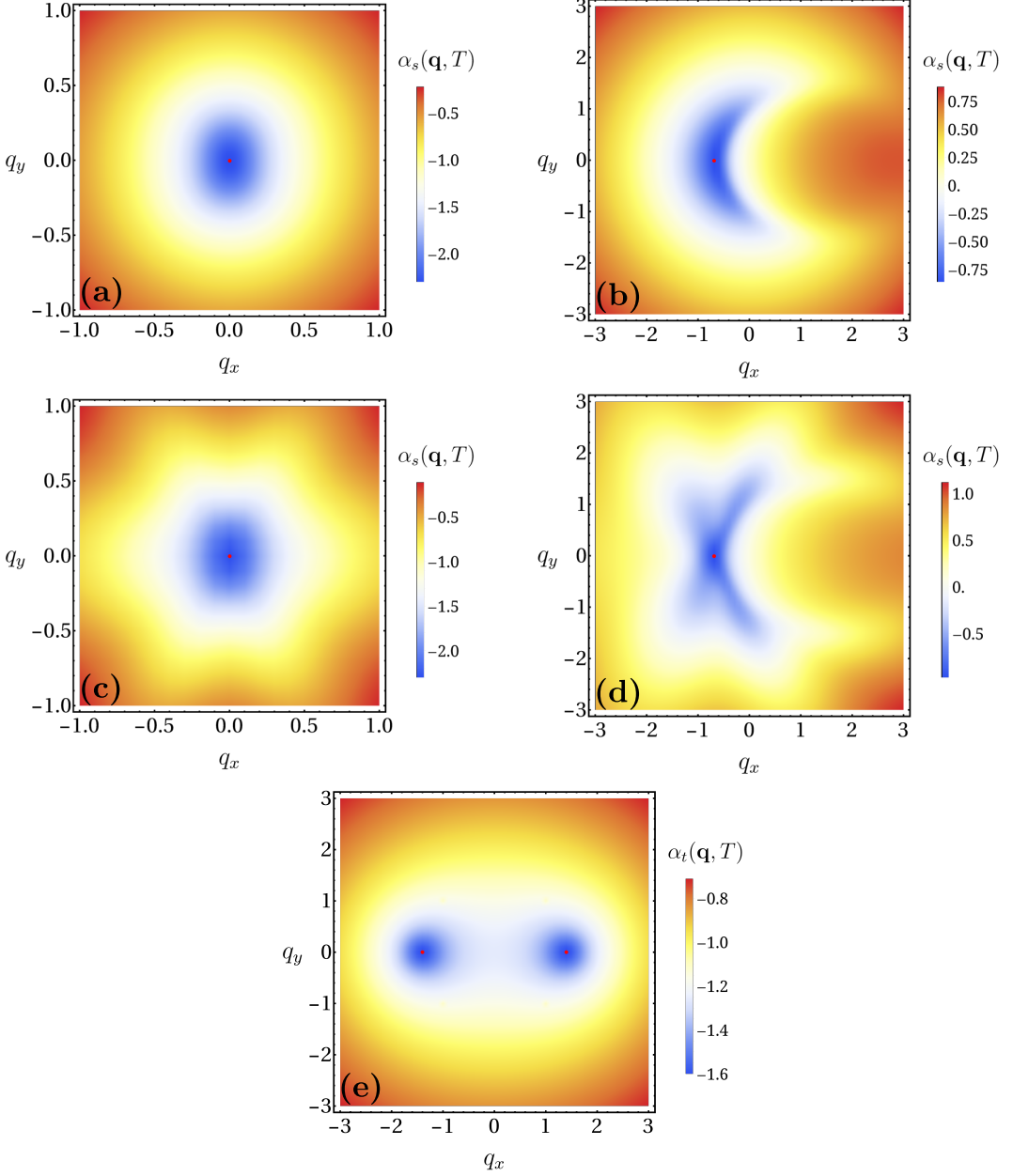


FIG. S1. Second-order coefficient of the GL free energy for the singlet [(a)-(d)] and triplet [(e)] pairing states with fixed temperature $T = 0.1T_{c,0}^{(s)}$ and splitting $\lambda/T_{c,0}^{(s)} = 1$. Upper panels (a) and (b) are for s -wave states with $B/T_{c,0}^{(s)} = 0$ and $B/T_{c,0}^{(s)} = 1$, respectively. In the latter case, note the emergence of a single nonzero minimum in the right panel, given by $\mathbf{Q} = -0.7\hat{\mathbf{x}}$. Bottom panels (c) and (d) are for d -wave states with $B/T_{c,0}^{(s)} = 0$ and $B/T_{c,0}^{(s)} = 1$, respectively. In the latter case, note the emergence of a single nonzero minimum in the right panel, given by $\mathbf{Q} = -0.7\hat{\mathbf{x}}$, so the only possible modulation is the FF one. Lower panel (e) is for helical p -wave state, showing the emergence of two minima $\pm\mathbf{Q}$, related by a C_{2z} rotation.

We now include the fourth-order term of the GL free energy, which is given by:

$$\delta\mathcal{F}^{(4)} = \frac{T}{2} \sum_{\mathbf{k}, i\omega_n} \sum'_{\substack{\mathbf{q}_1, \mathbf{q}_2 \\ \mathbf{q}_3}} \text{Tr} \left\{ G_0^{(p)}(\mathbf{k}) \hat{\Delta}^{(\mathbf{q}_1)} \left(\mathbf{k} - \frac{\mathbf{q}_1}{2} \right) \sigma_y G_0^{(h)}(\mathbf{k} - \mathbf{q}_1) \left[\hat{\Delta}^{(\mathbf{q}_2)} \left(\mathbf{k} - \mathbf{q}_1 + \frac{\mathbf{q}_2}{2} \right) \sigma_y \right]^\dagger G_0^{(p)}(\mathbf{k} - \mathbf{q}_1 + \mathbf{q}_2) \right. \\ \left. \hat{\Delta}^{(\mathbf{q}_3)} \left(\mathbf{k} - \mathbf{q}_1 + \mathbf{q}_2 - \frac{\mathbf{q}_3}{2} \right) \sigma_y G_0^{(h)}(\mathbf{k} - \mathbf{q}_1 + \mathbf{q}_2 - \mathbf{q}_3) \left[\hat{\Delta}^{(\mathbf{q}_1 - \mathbf{q}_2 + \mathbf{q}_3)} \left(\mathbf{k} - \frac{\mathbf{q}_1}{2} + \frac{\mathbf{q}_2}{2} - \frac{\mathbf{q}_3}{2} \right) \sigma_y \right]^\dagger \right\}, \quad (\text{S35})$$

where the prime in the summation above means that there is an additional constraint given by $\mathbf{q}_1 + \mathbf{q}_2 - \mathbf{q}_3 \in A$, where $A = \{\pm\mathbf{Q}\}$ is the set of minimization wave vectors. The calculation of these expressions can be summarized in terms of Feynman diagrams, which are shown in Fig. S2 for both FF (singlet and triplet) and LO (triplet) phases. We will

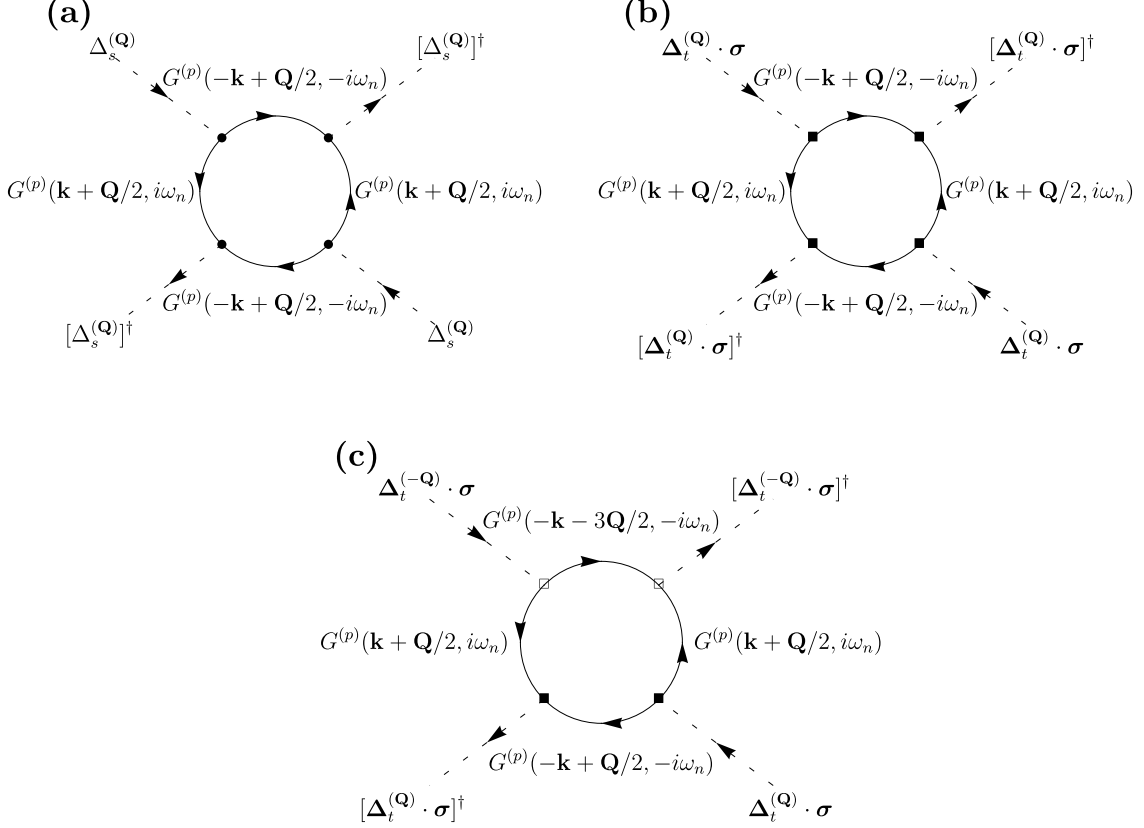


FIG. S2. Fourth-order Feynman diagrams for (a) spin-singlet FF, (b) spin-triplet FF and (c) spin-triplet LO order. The Feynman rules for the vertices are extracted from Eq. (S35) as: $\bullet \equiv d_0(\mathbf{k})\sigma_y$ for incoming external legs, $\bullet \equiv [d_0(\mathbf{k})\sigma_y]^\dagger$ for outgoing external legs, $\blacksquare \equiv \mathbf{d}(\mathbf{k}) \cdot \boldsymbol{\sigma} \sigma_y$ for incoming external legs, $\blacksquare \equiv [\mathbf{d}(\mathbf{k}) \cdot \boldsymbol{\sigma} \sigma_y]^\dagger$ for outgoing external legs, $\square \equiv \mathbf{d}(\mathbf{k} + \mathbf{Q}) \cdot \boldsymbol{\sigma} \sigma_y$ for incoming external legs and $\square \equiv [\mathbf{d}(\mathbf{k} + \mathbf{Q}) \cdot \boldsymbol{\sigma} \sigma_y]^\dagger$ for outgoing external legs. Since this is a pairing channel, the following similarity transformation $G^{(h)}(\mathbf{k}, i\omega_n) = -[G^{(p)}(-\mathbf{k}, -i\omega_n)]^T$ was used to derive these diagrams.

calculate these fourth-order coefficients below for the spin-singlet and spin-triplet pairing states, separately.

SINGLET PAIRING STATES

We first focus on spin-singlet pairing states by making $\mathbf{d}(\mathbf{k}) = 0$. For completeness, we consider both s -wave and d -wave pairing symmetries (for wave vectors in the vicinity of the Γ point), i.e., with form factors given by

$$d_0(\mathbf{k}) = 1 \Rightarrow s\text{-wave}, \quad (S36)$$

$$d_0(\mathbf{k}) = \frac{2\sqrt{2}}{k_F^2} k_x k_y \Rightarrow d_{xy}\text{-wave}. \quad (S37)$$

Consequently, we observe that only an FF phase can emerge upon the application of a magnetic field in these cases. Therefore, the only contribution that comes from the fourth-order coefficient is obtained by setting $\mathbf{q}_i = \mathbf{Q}$ (for $i = 1, 2, 3$) in Eq. (S35), or, equivalently, evaluating the Feynman diagram in Fig. S2(a), which yields:

$$\begin{aligned} \delta\mathcal{F}_{FF,singlet}^{(4)} = & |\Delta_s^{(\mathbf{Q})}|^4 T \sum_{\mathbf{k}, i\omega_n} d_0^4(\mathbf{k}) \left\{ \left[G^{(+)} \tilde{G}^{(+)} \right]^2 - 2G^{(+)} \tilde{G}^{(+)} G^{(-)} \tilde{G}^{(-)} \hat{\mathbf{g}}^{\text{eff}} \cdot \tilde{\mathbf{g}}^{\text{eff}} + \left[G^{(+)} \tilde{G}^{(-)} \right]^2 \right. \\ & - 2G^{(+)} \tilde{G}^{(-)} G^{(-)} \tilde{G}^{(+)} \hat{\mathbf{g}}^{\text{eff}} \cdot \tilde{\mathbf{g}}^{\text{eff}} + \left[G^{(-)} \tilde{G}^{(+)} \right]^2 \\ & \left. + \left[G^{(-)} \tilde{G}^{(-)} \right]^2 \left[(\hat{\mathbf{g}}^{\text{eff}} \cdot \tilde{\mathbf{g}}^{\text{eff}})^2 - (\hat{\mathbf{g}}^{\text{eff}} \times \tilde{\mathbf{g}}^{\text{eff}}) \cdot (\hat{\mathbf{g}}^{\text{eff}} \times \tilde{\mathbf{g}}^{\text{eff}}) \right] \right\} \equiv \chi_s(\mathbf{Q}) |\Delta_s^{(\mathbf{Q})}|^4, \end{aligned} \quad (S38)$$

where we have used the notation $\hat{\mathbf{g}}^{\text{eff}} \equiv \hat{\mathbf{g}}_{\mathbf{k} + \frac{\mathbf{Q}}{2}}^{\text{eff}}$ and $\tilde{\mathbf{g}}^{\text{eff}} \equiv \hat{\mathbf{g}}_{-\mathbf{k} + \frac{\mathbf{Q}}{2}}^{\text{eff}}$. The pairing phase diagram for the case of spin-singlet s -wave pairing is shown in the main text. Regarding the phase diagram for the case of spin-singlet d -wave pairing, its

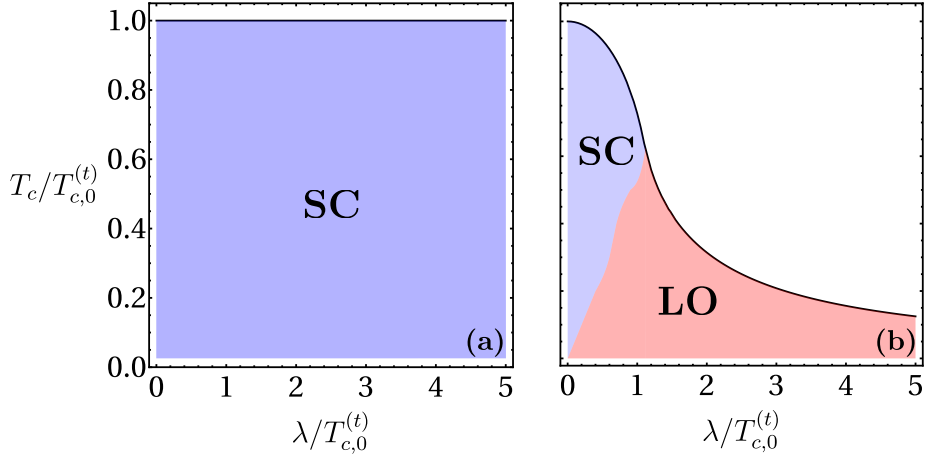


FIG. S3. Triplet critical temperatures of the chiral p -wave (a) and helical p -wave (b) pairing states as a function of the UPM splitting λ for zero magnetic field. Note that the chiral p -wave state is not affected by λ and also does not generate any finite-momentum superconductivity. An LO state only emerges in the case of a helical p -wave phase for finite λ . Although the latter state is suppressed by λ , this suppression is mild, since T_c only reaches zero in the limit $\lambda \rightarrow \infty$.

structure is similar to the pairing phase diagram for s -wave singlet states, with only a slightly smaller critical temperature compared to the latter.

TRIPLET PAIRING STATES

We now focus on the triplet states by making $d_0(\mathbf{k}) = 0$. As explained in the main text, we consider both helical p -wave and chiral p -wave pairing symmetries (for wave vectors in the vicinity of the Γ point), i.e., with form factors given by:

$$\mathbf{d}(\mathbf{k}) = i(k_x \hat{\mathbf{y}} + k_y \hat{\mathbf{x}}) \Rightarrow \text{helical } p\text{-wave}, \quad (S39)$$

$$\mathbf{d}(\mathbf{k}) = (k_x + ik_y) \hat{\mathbf{z}} \Rightarrow \text{chiral } p\text{-wave}. \quad (S40)$$

Here, we will concentrate on triplet pairing states satisfying the following condition:

$$\hat{\mathbf{g}}_{\mathbf{k}}^{\text{eff}} \cdot \left(\Delta_t^{(\mathbf{q}_i)}(\mathbf{k}) \times [\Delta_t^{(\mathbf{q}_i)}(\mathbf{k})]^* \right) = 0, \quad (S41)$$

which corresponds to unitary states. Note from Fig. S1(e) that we can have either one or two possible minimization wave vectors $\pm \mathbf{Q}$, so we need to evaluate the fourth-order coefficient for triplet states given in the Feynman diagrams shown in Figs. S2(b) and S2(c). Evaluating these diagrams, we get for the FF phase:

$$\begin{aligned} \delta \mathcal{F}_{FF, \text{triplet}}^{(4)} &= |\Delta_t^{(\mathbf{Q})}|^4 T \sum_{\mathbf{k}, \omega_n} \left([G^{(+)} \tilde{G}^{(+)}]^2 [2(\mathbf{d} \cdot \mathbf{d}^*)^2 - (\mathbf{d} \cdot \mathbf{d})(\mathbf{d}^* \cdot \mathbf{d}^*)] + 2[G^{(-)} \tilde{G}^{(+)}]^2 [(\mathbf{d} \cdot \mathbf{d})(\mathbf{d}^* \cdot \mathbf{d}^*)] \right. \\ &\quad + [G^{(-)} \tilde{G}^{(-)}]^2 [2((\hat{\mathbf{g}}^{\text{eff}} \cdot \mathbf{d})(\hat{\mathbf{g}}^{\text{eff}} \cdot \mathbf{d}^*) - (\hat{\mathbf{g}} \times \mathbf{d}) \cdot (\hat{\mathbf{g}}^{\text{eff}} \times \mathbf{d}^*))^2 - (\mathbf{d} \cdot \mathbf{d})(\mathbf{d}^* \cdot \mathbf{d}^*)] \\ &\quad \left. - 4G^{(+)} G^{(-)} \tilde{G}^{(+)} \tilde{G}^{(-)} (\mathbf{d} \cdot \mathbf{d}^*)(\hat{\mathbf{g}}^{\text{eff}} \cdot \mathbf{d})(\hat{\mathbf{g}}^{\text{eff}} \cdot \mathbf{d}^*) - (\hat{\mathbf{g}}^{\text{eff}} \times \mathbf{d}) \cdot (\hat{\mathbf{g}}^{\text{eff}} \times \mathbf{d}^*)] \right) \\ &\equiv \chi_t^{\text{FF}}(\mathbf{Q}) |\Delta_t^{(\mathbf{Q})}|^4, \end{aligned} \quad (S42)$$

where $\mathbf{d} \equiv \mathbf{d}(\mathbf{k})$. For the LO phase, two copies of the diagram in Fig. S2(b) appear, one corresponding to $+\mathbf{Q}$ and the other to $-\mathbf{Q}$, and other four expressions appear corresponding to the diagram in Fig. S2(c). Using the corresponding

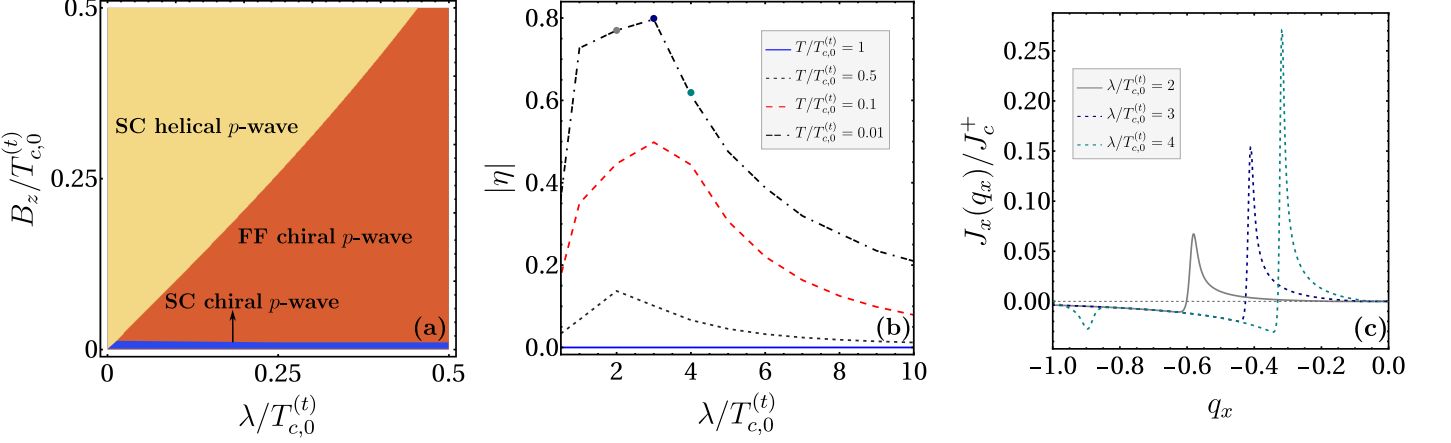


FIG. S4. (a) Schematic pairing phase diagram of B_z vs. λ in the present model for spin-triplet superconducting states. (b) Efficiency η of the SDE for the chiral p -wave FF phase with modulation along the direction of the minimizing wave vector \mathbf{Q} , as a function of the UPM spin splitting λ for a finite magnetic field such that $B_z/T_{c,0}^{(t)} = 1$. We also show the behavior of η in the model for different temperatures T . (c) Supercurrent as a function of the momentum q_x for different values of the spin splitting around the maximum of the efficiency, indicated by three circles shown in (b), at $T = 0.01T_{c,0}^{(t)}$.

Feynman rules, we obtain:

$$\begin{aligned}
\delta\mathcal{F}_{\text{LO},\text{triplet}}^{(4)} &= \chi_t^{\text{FF}}(\mathbf{Q})|\Delta_t^{(\mathbf{Q})}|^4 + \chi_t^{\text{FF}}(-\mathbf{Q})|\Delta_t^{(-\mathbf{Q})}|^4 \\
&\quad + 4|\Delta_t^{(\mathbf{Q})}|^2|\Delta_t^{(-\mathbf{Q})}|^2T \sum_{\mathbf{k},\omega_n} \text{tr} \left\{ \left(G^{(+)}\sigma_0 + G^{(-)}\hat{\mathbf{g}}_{\mathbf{k}+\frac{\mathbf{Q}}{2}}^{\text{eff}} \cdot \boldsymbol{\sigma} \right) \mathbf{d}(\mathbf{k}) \cdot \boldsymbol{\sigma} \sigma_y \right. \\
&\quad \left(\tilde{G}^{(+)}\sigma_0 + \tilde{G}^{(-)}\hat{\mathbf{g}}_{-\mathbf{k}+\frac{\mathbf{Q}}{2}}^{\text{eff}} \cdot \boldsymbol{\sigma} \right) [\mathbf{d}(\mathbf{k}) \cdot \boldsymbol{\sigma} \sigma_y]^\dagger \left(G^{(+)}\sigma_0 + G^{(-)}\hat{\mathbf{g}}_{\mathbf{k}+\frac{\mathbf{Q}}{2}}^{\text{eff}} \cdot \boldsymbol{\sigma} \right) \mathbf{d}(\mathbf{k}+\mathbf{Q}) \cdot \boldsymbol{\sigma} \sigma_y \\
&\quad \left. \left(G'^{(+)}\sigma_0 + G'^{(-)}\hat{\mathbf{g}}_{-\mathbf{k}-\frac{3\mathbf{Q}}{2}}^{\text{eff}} \cdot \boldsymbol{\sigma} \right) [\mathbf{d}(\mathbf{k}+\mathbf{Q}) \cdot \boldsymbol{\sigma} \sigma_y]^\dagger \right\} \\
&= \chi_t^{\text{FF}}(\mathbf{Q})|\Delta_t^{(\mathbf{Q})}|^4 + \chi_t^{\text{FF}}(-\mathbf{Q})|\Delta_t^{(-\mathbf{Q})}|^4 + 4|\Delta_t^{(\mathbf{Q})}|^2|\Delta_t^{(-\mathbf{Q})}|^2\chi_t^{\text{LO}}(\mathbf{Q}),
\end{aligned} \tag{S43}$$

where we have used the notation $G^{(\pm)}(\mathbf{k} + \frac{\mathbf{Q}}{2}) \equiv G^{(\pm)}$, $G^{(\pm)}(-\mathbf{k} + \frac{\mathbf{Q}}{2}) \equiv \tilde{G}^{(\pm)}$ and $G'^{(+/-)} \equiv G'^{(+/-)}(-\mathbf{k} - \frac{3\mathbf{Q}}{2}, -i\omega_n)$.

We are now able to determine whether the emergent PDW phase in Fig. S1(e) is an FF or an LO phase, by checking which has the smaller free energy. The analysis of energetics within the GL theory reveals that for the helical p -wave state, the stable phase is the LO phase, as shown in Fig. S3(b). Note, however, that the chiral p -wave phase is unaffected by the UPM spin splitting, whereas the helical p -wave state is mildly suppressed. The corresponding triplet pairing phase diagram is displayed in Fig. S4(a), where we have obtained which pairing phase has the highest critical temperature, revealing the dominant order. As a result, the LO pairing phase is not present in the phase diagram in Fig. S4(a).

SUPERCONDUCTING DIODE EFFICIENCIES

In this last section, we turn our attention to the SDE efficiencies in our model for the additional pairing symmetries investigated in this work. As explained in the main text, only the FF state will lead to a finite intrinsic diode efficiency η , since this pairing phase breaks both time-reversal and inversion symmetries. For this reason, in Fig. S5, we show the corresponding efficiency for spin-singlet d -wave FF state in the presence of a finite magnetic field. As a result, we observe that the SDE efficiency in this case yields smaller values than the s -wave FF case, which was discussed in the main text.

In Fig. S4(b), we show the corresponding efficiency for the chiral p -wave FF state. Note that this quantity is quantitatively similar to the efficiencies obtained for the spin-singlet s -wave FF state explained in the main text: Indeed, we observe here that the SDE efficiency also has a peak for low temperatures at an optimal splitting, which can reach almost 80% of efficiency for some conveniently chosen physical parameters. We also point out that the SDE efficiency in this case exhibits a tendency to increase as the temperature decreases. Finally, in Fig. S4(c), the supercurrents are plotted at $T = 0.01T_{c,0}^{(t)}$ as a function of the component of the wave vector q_x , which refers to the direction of modulation \mathbf{Q} that produces the highest SDE efficiencies.

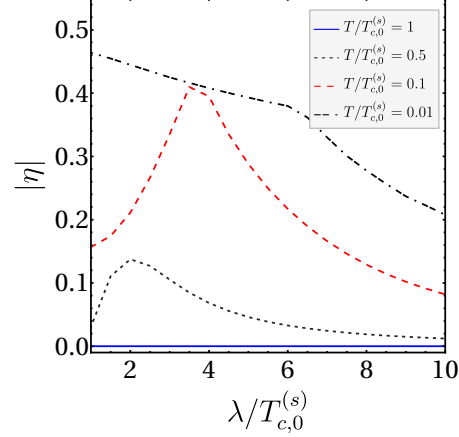


FIG. S5. Efficiency η of the SDE for the spin-singlet d -wave FF phase with modulation along the direction of the minimizing wave vector \mathbf{Q} , as a function of the UPM spin splitting λ for a finite magnetic field such that $B_z/T_{c,0}^{(s)} = 1$. We also show the behavior of η in the model for different temperatures T .